2005

Characterization of L-cysteine Thin Films Via Photoemission Spectroscopy

Roy Gargagliano
University of South Florida

Characterization of L-cysteine Thin Films Via Photoemission Spectroscopy

by

Roy Gargagliano

A thesis submitted in partial fulfillment
of the requirements for the degree of
Master of Science in Electrical Engineering
Department of Electrical Engineering
College of Engineering
University of South Florida

Major Professor: Rudy Schlaf, Ph.D.
John T. Wolan, Ph.D.
Francis Moussy, Ph.D.

Date of Approval:
November 1, 2005

Keywords: XPS, UPS, interface, amino acid, electronic structure

Dedication

To my wife, Melissa, for her constant support of my education and her example to me of how to succeed in life. To Dr. Schlaf for giving me the opportunity to engage in research at the undergraduate level and for inspiring me to pursue a graduate degree.

Acknowledgements

I would like to thank Dr. Martin Beerbom and Dr. Rudy Schlaf for their advice and instruction. Financial support from the National Science foundation and the Petroleum Research Fund is gratefully acknowledged.

Table of Contents

List of Tables

List of Figures

Characterization of L-cysteine Thin Films Via Photoemission Spectroscopy

Roy Gargagliano

ABSTRACT

Using photoemission spectroscopy (PES) the interface between the amino acid L-cysteine and a Au substrate was characterized to determine its electronic and chemical structure. L-cysteine was deposited on a Au substrate in several experiments via dipping into solution or via evaporation. The depositions were performed in several steps. Between deposition steps x-ray photoemission spectroscopy (XPS) and ultraviolet photoemission spectroscopy (UPS) measurements were taken. XPS was used to characterize the chemical interaction at the interface while UPS was used to determine the orbital line-up at the interface and the highest molecular orbital (HOMO) structure of L-cysteine. The results indicate the formation of an interface state at approximately 1.5 eV above the L-cysteine HOMO.

Introduction

Increased interest in bioengineering has sparked investigation into organic/inorganic interfaces. Of particular interest are protein/inorganic interfaces. Proteins selectivity and affinity for molecular recognition makes them especially useful for bioengineering applications such as biosensors [1]. The applications of such protein based biosensors are widespread including detection of heavy metals [2], glucose sensing and microbal warfare agent detection [3], and detection of Domic acid [4]. A method of using L-cysteine monolayers as a wetting agent to reduce clogging of inkjet nozzles was recently patented [5].

Large complex molecules provide many options for such functions but their complexity impedes evaluation of the interface. The functional characterization of these molecules should start with simple molecules which provide the opportunity to evaluate the interface with the fewest variables. Knowledge gained in such experiments can be used for later evaluation of more complex molecules which may provide a greater range of functionality. As the molecular units which make up proteins amino acids provide a good choice for these initial investigations.

The amino acid L-cysteine provides an excellent opportunity to examine these interfaces. L-cysteine's thiol group allows it to covalently bond to transition metals and produce a stable and well ordered self assembled monolayer (SAM). The stability and chemical tolerance of such SAMs makes them excellent candidates for device manufacture. As a large amino acid L-cysteine can provide a mechanism to connect larger proteins to a metal substrate as shown in Ref. [6]. L-cysteine has been shown to adhere to a range of metals such as Cu, Au, Ag, and Ni; References [7, 8] provide two examples of work done on these interfaces. The simpler molecule and monolayer present an interface that is easier to characterize than a larger molecule and/or multiple layers.

The thin films produced by dipping metal surfaces into L-cysteine solutions provide an interface that is not buried by a significant number of molecular layers. This

is particularly important for surface sensitive techniques such as x-ray photoemission spectroscopy (XPS) and ultraviolet photoemission spectroscopy (UPS). The thin films produced do not significantly interfere with attempts to measure the interface. UPS provides a technique which allows characterization of the interface specifically determination of the charge injection barrier and interface dipole. XPS provides a view of the chemical interaction at the interface and the molecule itself.

Photoemission spectroscopy (PES), of which UPS and XPS are specific examples, provides direct measurement of the interface without the construction of special devices or modification of the sample. Its surface sensitivity provides a built in limitation that results in measurement of the SAM and interface but very little of the bulk substrate. As PES is conducted inside high vacuum environments contamination during measurement is minimized. The low energy radiation typically used in XPS is less damaging to organic materials than other techniques though the potential for damage should not be ignored.

L-cysteine/Au interface properties have been reported in several papers including theoretical evaluation of the interface, [9, 10]; deposition via solution, [8, 11-14], and deposition via evaporation[15]. All of the papers involving solutions expose the sample to atmosphere during transfer from the solution to vacuum increasing the potential for contamination. These works generally agree on the binding energies resulting from the interface and the morphology of the resulting monolayer.

Those works present measurements taken after a single step evaporation or dip in solution, usually 24 hours. They view the completed interface and cannot see changes as it forms. In the experiments for this study depositions were performed in steps so that the formation of the interface could be measured. Clean samples were exposed for a short time (via solution or evaporation) and then measured via PES. The samples were then exposed for a slightly longer time and subsequently measured. The process of exposure then measurement is repeated for several steps.

This multi-step process allowed evaluation of the electronic interface, detection of emission shifts during SAM formation, and detection of x-ray damage. An analogy can be drawn to taking the picture of a completed house (in the case of previous work) and

taking several pictures of the building as construction proceeds (this study). Multiple pictures present the foundation being poured, framing of the home, and the guts of the house where as the single picture obscures all this information. This study also presents ultraviolet electron spectroscopy (UPS) measurements of the interface, as no other group has presented such results these results add to the body of work.

Some recent papers implementing this multi-step process include the evaluation of the work function of indium tin oxide films [16], investigation of the band lineup of p- and n-type 4H-SiC/Al [17] and 4H-SiC/Ni [18] interfaces, determination of the charge injection barriers at a ribonucleic acid/HOPG interfaces [19], investigation of luminescent polymer thin films [20], and previous publication of the dipping results discussed in this study [21]. These papers demonstrate the capability of PES to facilitate evaluation of the electronic structure of an interface and the effectiveness of multi-step deposition and measurement cycles in determining growth morphology, interface chemistry, and evaluating the electronic structure.

Self Assembled Monolayers (SAM) and L-cysteine SAMs

Self assembled monolayers (SAM) are the result of spontaneous formation of ordered structures by molecules adsorbing upon a substrate. The components necessary for this to occur are a solid or liquid substrate and a molecule which has a functional group that has an affinity for the substrate.

Figure 1 from Ref. [22] shows a basic model of a SAM where molecules have bonded to the substrate. The headgroup is the functional group that has an affinity for the substrate. The endgroup is the group that exists at the opposite end of the molecule. It determines many of the properties of the monolayer as it is the portion of the SAM that is available to bond to other molecules. The backbone is essentially the rest of the molecule. Its interaction with the other molecules will determine the angle of the molecule in the monolayer and the molecule's rotation.

SAMs formed from organic molecules are of particular interest in research and industry as organic components can often be adjusted by replacing a particular group (usually the endgroup) without having to change the other portions of the molecule. A

specific example is how changing the endgroup of alkylthiol molecules from –OH to –CH_3 will change the monolayer from hydrophillic to hydrophobic [22]. Conversely the headgroup can be changed to provide stronger or weaker bonds for specific purposes.

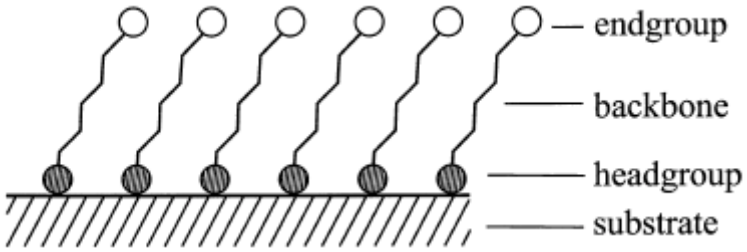

Figure 1: Basic Model of Self Assembled Monolayers; Showing a Molecule Whose Headgroup has an Affinity for Binding to a Substrate

SAMs can be formed from a variety of materials and via a variety of methods. Some materials that can be used to form SAMs include long-chain n-alkanoic acids ($C_nH_{2n+1}COOH$) on transition metals like Ag, Cu, and Al or AlO_3; alkylchlorosilanes, alkylakoxysilanes, and alkylamaniosilanes on hydroxylated surfaces; organosulfur adsorbates on metals or semiconductors such as alkanethiolates on Au; and alkyl chains on Si [23].

Figure 2 from Ref [22] shows methods by which thin films can be formed. On the top of Figure 2 a SAM is formed by dipping the substrate into a solution of the appropriate molecule and at the bottom the SAM is formed by evaporation of the material in ultra high vacuum (UHV). SAMs formed from molecules containing a thiol group (-SH) on Au have been identified as model systems for investigation [24].

Thiol based monolayers also provide advantages in research due to their ease of preparation and stability of the monolayer. In addition, thiol molecules bond to a great many organic and inorganic surfaces allowing for a great many potential applications. Of particular interest are the transition metals, such as Ag, Cu, Ni, and Au. Though thiols will bond to any Au configuration Au (111) surfaces are preferred for most SAM research as they are easy to prepare via evaporation. It is expected that many practical

applications will likely use such evaporated surfaces, which result in predominantly (111) surfaces, rather than single crystals [22, 25]. The well defined order of the resulting substrate and the relative inertness of gold provide additional support for this preference especially in cases where surface imaging techniques are used or a sample is exposed to atmosphere.

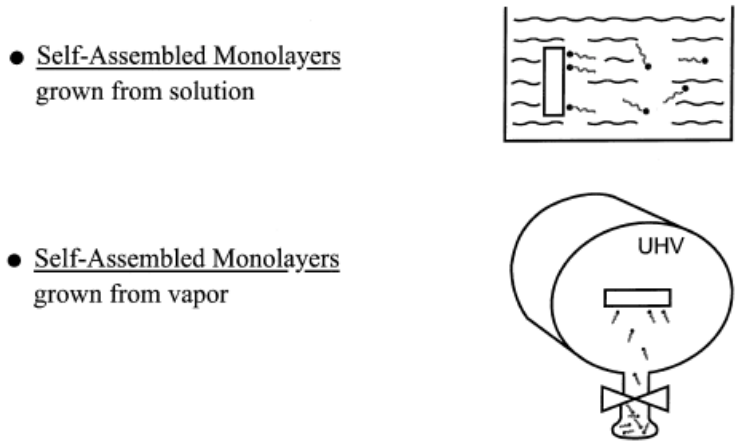

Figure 2: Preparation Methods for Organic Layers

When binding to Au, hydrogen disassociates from the thiol and sulfur forms a covalent bond with the Au [15, 23]. The adsorption of the thiol from solution is thought to occur in a two or three step process [22, 23]. The first step is quick, measured in minutes, and produces a layer near maximum thickness and final contact angles. The second step, measured in hours, ends with the layer at full thickness and at the final contact angles. In some cases it has been found that on a timescale on the order of days there is rearrangement of molecules from many smaller islands or groups to fewer islands. The duration of the first step depends on concentration and determined the selection of solution concentrations in the dipping experiments described below.

Several phases and two molecule orientations have also been shown to exist during formation of a SAM. The two orientations are lying down and standing up. Laying down occurs as molecules first adsorb to the substrate. During laying down the first phase is a very low coverage or "lattice gas" phase where very few molecules are

adsorbed to the substrate. As coverage increases a striped phase occurs where the molecules are oriented in such a way that striped islands can be clearly seen during scanning tunneling microsopy (STM). The third phase is intermediate structures which still show as striped with STM, where la,ying down molecules begin to stack upon each other. Two intermediate structures have been reported [22] and are noted in Figure 3 from the same reference. At some point enough molecules are adsorbed that other molecules are forced to a more erect position. At this point the SAM is in the standing phase. Figure 3 shows a schematic of these phases from work with decanethiol on Au, A and B showing the initial striped phases; C and D are intermediate phases, and E shows the standing phase.

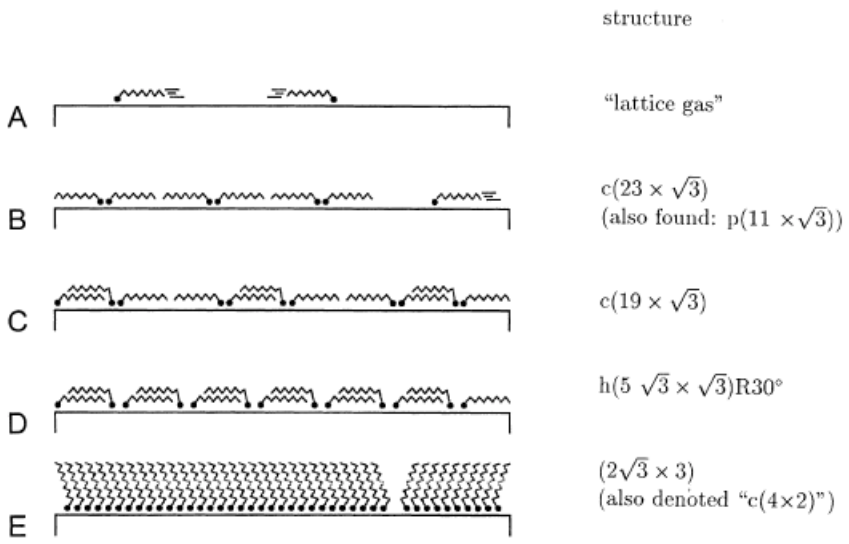

Figure 3: Phases of SAM Formation; A and B are Striped Phases, C and D Represent Intermediate Phases, and E is the Standing Phase

Figure 4 shows a similar progression of mercaptohexanol evaporated on Au(111). The top left image is the herring bone of clean Au(111). B shows a small island of striped phase and C shows these islands increasing in size. In D the islands show a significant amount of coverage. In E the bright areas represent small islands of standing molecules while the dark areas are striped phase portions. Finally, in F the standing

phase portions cover a significant portion and continue coverage until no appropriate bond sites are available.

The dark holes in Figure 4 represent Au vacancy islands. These holes are observed very early and become more prominent as the monolayer forms. It has been shown that some Au ends up in the solution when SAMS are formed via dipping [23, 25] but as Figure 3 shows the vacancies also occur with evaporation. The Au found in the solutions is also not enough to explain the holes. Some theories have been proposed for these holes such as substrate reconstruction or weakening of Au-Au bonds due to the thiolate bonds. So far the mechanism behind these holes has not been adequately explained.

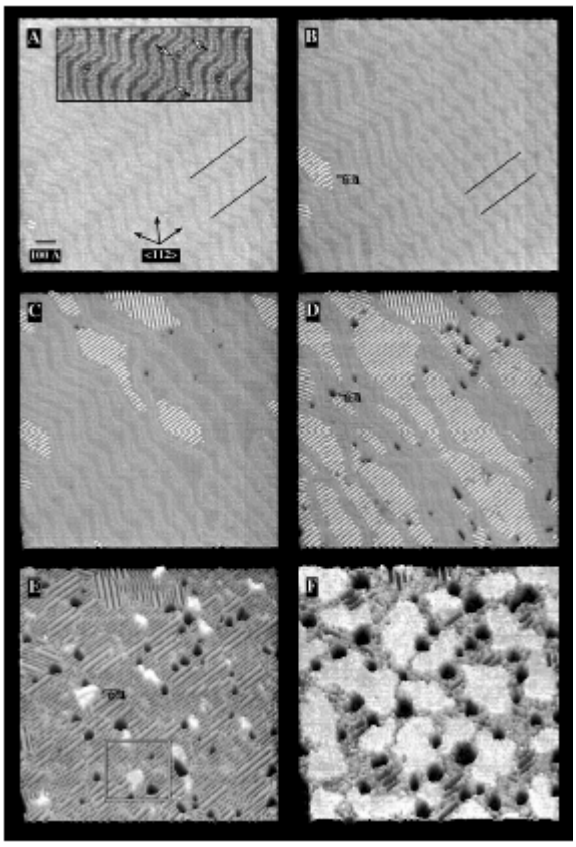

Figure 4: Constant Current STM Images. A is Clean Au(111), B Through D Show Striped Phases, E and F Show Standing Phase, from Ref. [22]

It is has been shown that thiols on Au(111)bond at every sixth hollow site producing a $\sqrt{3}x\sqrt{3}$ R30° lattice for the monolayer repeating the hexagonal structure of the substrate lattice. Ulman [23] has proposed that thiols first adsorb to Au atoms adjoining the hollows and that scission of the S-H bond occurs at this point. The thiols then move to the hollow forming ordered domains. However, recent work with methanethiolate lattices has shown them to adsorb at the on top sites around the hollows [25]. DFT studies indicate that the adsorption energy for the on top sites is the least favorable.

L-cysteine's thiol group makes it interesting for the examination of SAMs. L-cysteine, $C_3H_7NO_2S$, is the naturally occurring form of the amino acid Cysteine. Cysteine is implicated in various biological functions such as enzyme activities and the building up of protein structures. As a relatively simple molecule it is a good option for investigating the formation and structure of monolayers . Uvdal [15] proposed a structure for L-cysteine monolayers on Au Figure 5 shows an extended example. An initial layer of chemisorbed molecules bonds covalently to the Au vial the thiol group forming a gold thiolate. A second layer is physisorbed upon that first layer and held in place via Vanderwalls forces.

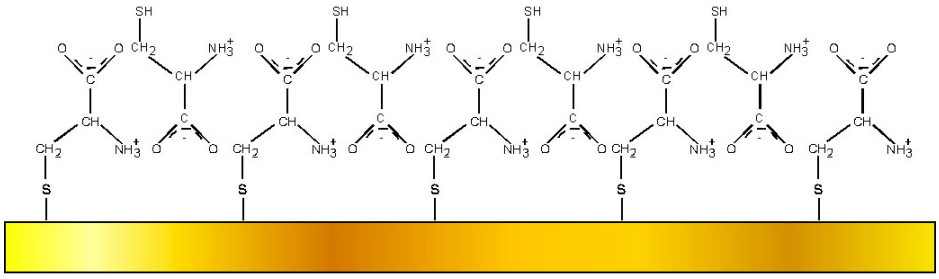

Figure 5: Proposed Structure of L-cysteine Monolayers on Au, After Uvdal et al

The advantages of PES techniques make them quite suited to investigation of SAMs. They allow direct measurement of an unmodified sample and the surface sensitivity of the technique is a significant advantage in such studies.

Photoelectron Spectroscopy

Photoelectron spectroscopy (PES) utilizes the photoelectric effect in order to characterize a particular sample including its electronic structure and elemental composition. In the photoelectric effect a photon ionizes an electron from a molecule. Any energy in excess of that required to ionize the electron imparts kinetic energy to that electron. In PES electrons of a specific kinetic energy can be counted. Performing this count operation over a spread of energies produces a spectrum which can be used to characterize a sample.

PES is typically divided by the source of ionizing photons. The most common sources are x-ray and ultraviolet. X-ray photoelectron spectroscopy (XPS) utilizes soft x-rays in the 200-2000 eV range. These energy levels allow examination of the core electron levels. Ultraviolet photoelectron spectroscopy (UPS) utilizes vacuum UV radiation in the 10-45 eV range. These energy levels allow examination of the valence electron levels.

Physical Basis

The photoelectric effect was discovered by Heinrich Hertz in 1887 who found that the spark on a secondary arc was more pronounced if it was not shielded from the light produced by a driving arc. With a little more investigation he found that the ultraviolet light produced by the driving arc was the cause. Hertz investigated the phenomenon no further and merely noted the results.

Investigation by others led to the conclusion that the light was causing electrons to be ejected by exciting the electrons. The wavelength of the light was also found to affect the energy of the ionized electrons. Shorter wavelength, higher energy, light increased the speed of the electrons and higher intensity caused more electrons to be ionized. In 1905 Einstein proposed an explanation [26] involving the quantum properties of light. An important result was the idea that the energy from a photon could not be partially absorbed. So a photon impinging upon an electron transferred all its energy. If that energy was sufficient the electron could ionize to the vacuum level.

An equation to find kinetic energy of an electron reaching the vacuum level can be easily derived starting with the energy of a photon,

$$E=h\upsilon \qquad (1.)$$

where E is energy, h is Plank's constant and υ is the frequency of light. If a photon impinges upon an electron, e^-, in a molecule, M, and that photon imparts enough energy to ionize the electron to the vacuum level we have the following process:

$$M + h\upsilon \rightarrow M+ + e-, \qquad (2.)$$

this process ignores any conservation of energy as the ionized electron was imparted enough energy to overcome its bonds and any attraction of the molecule to get to the vacuum level. The electron will also have a kinetic energy greater than or equal to zero. To account for the conservation of energy we can convert the process to an equation relating functions of energy, E,

$$E(M) + h\upsilon = E(M^+) + E(e^-). \qquad (3.)$$

The energy of the ionized electron is realized in kinetic energy, KE, so $E(e^-)$ can be replaced with KE. Since we are interested in the KE of the electron for the purpose of PES we can rearrange the equation to produce the following:

$$KE = h\upsilon + E(M) - E(M^+). \qquad (4.)$$

$E(M^+)$ represents the molecule's original energy plus the additional positive attraction that had been neutralized by the now ionized electron. That positive attraction represents the binding energy, BE, of the electron,

$$BE = E(M^+) - E(M). \qquad (5.)$$

Rearrangement of (4) produces,

$$KE = h\upsilon - [E(M^+) - E(M)], \qquad (6.)$$

which allows us to substitute (5) into (6) resulting in a final equation of

$$KE = h\upsilon - BE. \qquad (7.)$$

For the purposes of the photoelectric effect equation (7) is sufficient but for PES a correction must be made to account for the experimental method.

XPS and UPS measurements are usually represented on a binding energy scale with a zero point at the Fermi level. The Fermi level sits between the highest occupied molecular orbital (HOMO) and the vacuum level. The energy difference between the

vacuum level and the Fermi level is called the work function, Φ. This changes the way the binding energy is measured and changes equation (7) to the following:

$$KE = h\upsilon - BE - \Phi. \qquad (8.)$$

So equation (7) is a general equation for the kinetic energy of a photoemitted electron while equation (8) is the equation for the kinetic energy of a photemitted electron counted for PES.

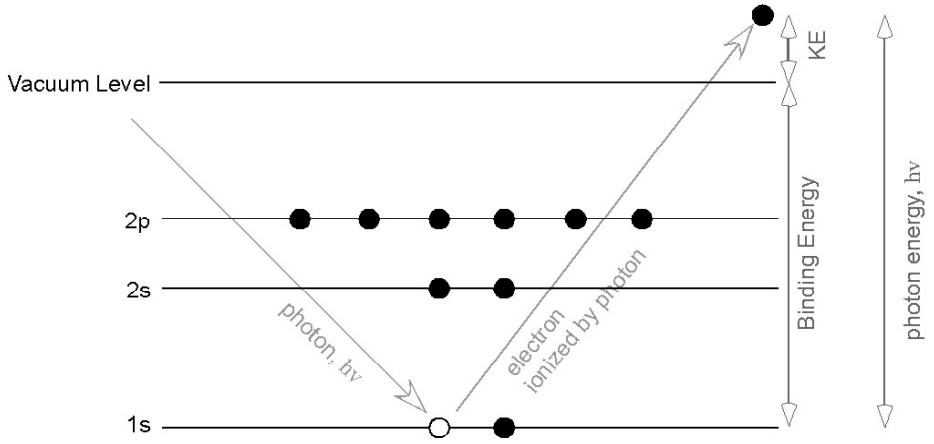

Figure 6: Photoelectric Effect for a Model Atom

Figure 6 presents the photoelectric effect in a model atom. A photon impinges upon an electron in the 1s orbital in the 1s orbital and imparts enough energy to ionize that electron. The loss of the electron produces a positively charged hole represented by the white circle. To the right the components of (7) can be seen where the photon energy equals the total of the binding energy and the kinetic energy.

Figure 7 presents the same principle but with the same photon impinging upon an electron in another orbital level, 2p. Since the 2p orbital represents a lower binding energy the resulting kinetic energy is greater. The lines to the right graphically show the resulting kinetic energies. Due to the difference in binding energy between the 2p and 1s orbitals the kinetic energy is greater for the 2p as its binding energy is smaller.

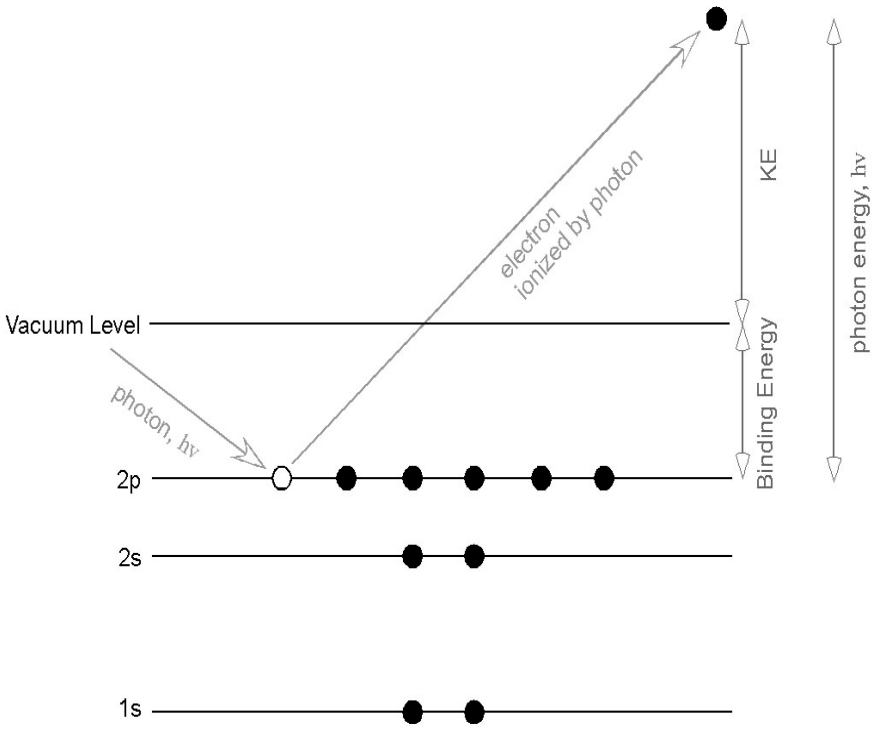

Figure 7: Photoelectric Effect for a Model Atom at 2p Orbital

A secondary effect of the photoemission is that an electron at a lower binding energy may move an inner orbital. This occurs approximately 10^{-14} seconds after the initial photoelectric event [27]. As energy must be conserved the difference in binding energies is emitted as a photon with

$$h\upsilon = BE_A - BE_I, \qquad (9.)$$

where BE_I is the binding energy of the ionized electron and BE_A is the binding energy of the electron replacing it. This secondary photon may then cause another electron to be ionized. This second electron is called an Auger electron. That electron's kinetic energy is equal to the difference between the energy of the initial ion (just after the photoelectric event) and the final doubly charged ion. The energy of the Auger electron is independent of the initial photon energy.

Figure 8 shows how an Auger electron is emitted as a model ion relaxes. An electron in the L2,3 orbital drops, line A, to the hole caused by the initial photoemission (Figure 6 or Figure 7). That electron emits a photon which causes a second electron to

ionize, line B. Auger electrons are usually referenced by the orbitals involved in the process so the example in Figure 8 would be a $KL_{23}L_{23}$ electron or more commonly KLL.

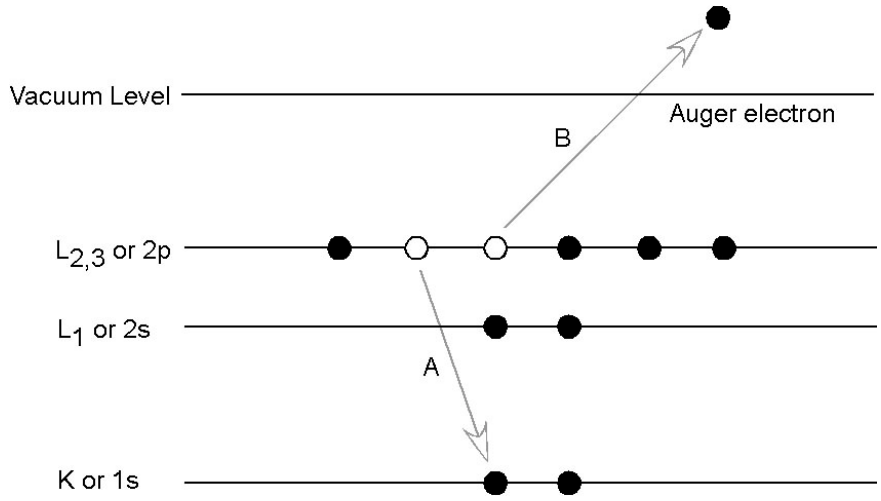

Figure 8: Auger Effect for a Model Atom

PES Equipment

The important work in PES was conducted by Kai Siegbahn and his coworkers who expanded it to examine non-metals and liquids and gases. Starting in the late 1950's and into the 1960's they developed Electron Spectroscopy for Chemical Analysis or ESCA [28]. ESCA was essentially PES but that group saw the first applications as most beneficial to the study of chemistry. The basic device consists of a fixed energy radiation source, a sample, an analyzer, an electron detector, and a high vacuum environment. Figure 9 presents a simplified schematic of a modern PES system.

The photon source is typically an x-ray or ultraviolet (UV) discharge lamp. The x-ray source is used to perform PES measurements on core electrons whereas the UV source is used to perform measurements on valence electrons. The x-ray source used for the experiments in this study was a Mg Kα ($h\upsilon$ = 1235.6 eV). For the valence electrons the UV light sources used have an upper range of 45 eV, for this study He I ($h\upsilon$ = 21.22 eV) was used.

An analyzer guides electrons of the desired energy to the electron detector and filters out electrons of other energies. Magnetic or electric fields are set at such energy that only an electron of the selected energy with be appropriately deflected and go to the electron detector. Those outside that energy range will be deflected into the walls of the analyzer and absorbed.

A spherical deflection analyzer (SDA) consists of two concentric hemispheres as shown in Figure 9. A photon source (x-ray or UV) impinges upon the sample and releases electrons via the photoelectric effect. Prior to entry to the analyzer the electron optics optimize the type of electrons coming into the entry slit. A physical aperture is the first obstacle. Changing the diameter of the opening changes the maximum angle at which an electron can enter the optics. The angle increases with diameter and more electrons through improving the signal but decreasing the resolution. The reverse is also true. Due to the high intensity of the UV produced by the gas discharge lamp it is typically necessary to set the aperture to the minimum value during UPS measurements. For XPS measurements the aperture was usually set in one of the larger diameters.

Next is a retardation stage prior to entry into the analyzer. The level of the retardation is referred to as the pass energy. This retardation acts as a high pass filter removing low energy electrons which primarily serve to increase noise. This pass energy is held fixed to maintain a constant resolution. The overall result is an increase in resolution which can be on the order of a 100x for valence band electrons [29].

After passing through the retardation stage an electron moves into the analyzer. The transmission of electrons is accomplished by changing the potential of the hemispheres. The voltage required is a function of the radii of the inner and the outer hemispheres and the energy desired. The equations, taken from [29], are as follows:

$$V_{out} = E_0 \times [3 - 2(R_0 / R_{out})] \text{ and} \qquad (10.)$$

$$V_{in} = E_0 \times [3 - 2(R_0 / R_{in})] \qquad (11.)$$

where V_{in} and V_{out} are the inner and outer potentials, E_0 is the initial energy of the electron coming through the entrance slit, $R_0 = (R_{in} + R_{out})/2$. The V_{in} and V_{out} potentials are adjusted to select all binding energies desired and produce a spectrum.

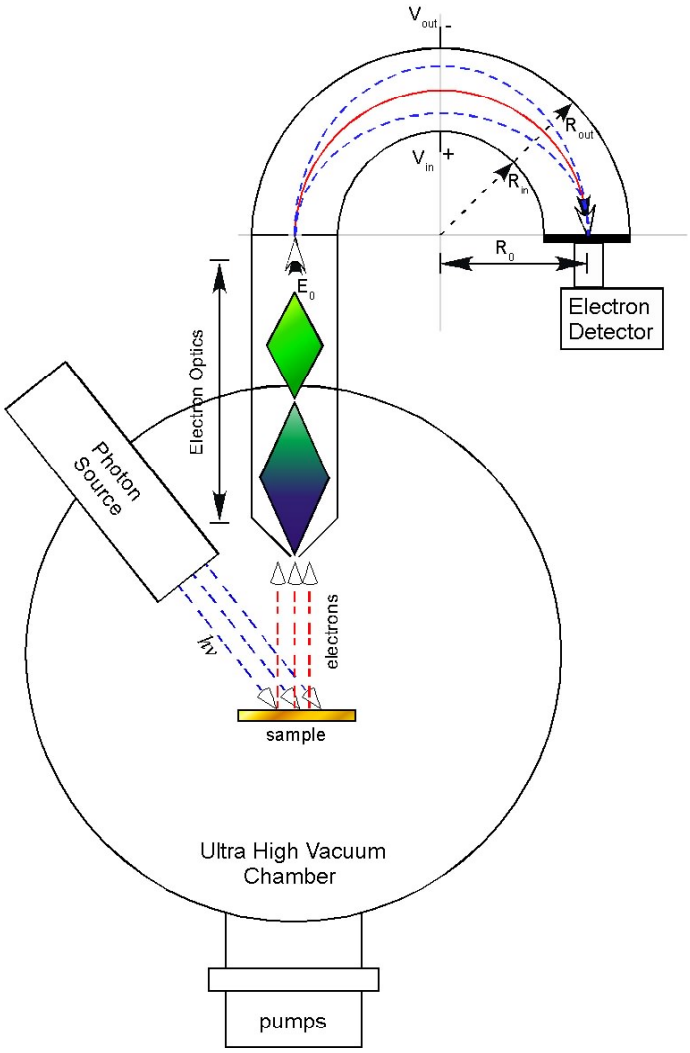

Figure 9: Photoemission Spectroscopy Equipment Schematic

Once an electron has passed through the analyzer it comes to the electron detector either an electron multiplier tube (used for this study) or a micro-channel detector. In order to measure electrons a detector uses a voltage and an electron's initial energy to produce a cascade of electrons which can then be measured or displayed. An electron strikes the detector wall with its initial energy plus the additional energy from the voltage present. It then ejects several electrons from the wall, those electrons gain energy from the voltage and each eject several electrons from the opposite wall further down the

detector than where the original electron struck. This effect continues until a large number of electrons, on the order of thousands, are brought to the end of the detector and measured.

The measured electrons have a kinetic energy given by:

$$KE = h\upsilon - BE - \Phi_s \quad (12.)$$

where Φ_s is the work function of the spectrometer. The important result of this equation is that knowledge of the sample's work function as shown in equation (8) is not required to gain the binding energy. The elimination of the sample's work function is accomplished by Fermi level referencing which is accomplished via a common ground and confirmed via calibration. This is accomplished by calibrating the analyzer with a peak in Au, Cu, or Ag. Use of multiple standards further confirms the position of the energy scale and its linear accuracy.

A sample holder provides a ground to prevent charging of the sample. If the ejected electrons are not replaced then the sample will begin to have a positive charge and the energy required to eject subsequent electrons will increase with exposure time. The ground also serves the purpose of allowing Fermi level referencing as discussed above.

A vacuum chamber capable of providing at least high vacuum provides a method of keeping a sample clear of contamination long enough to complete measurements. Outside of a vacuum a sample acquires enough contamination to significantly affect readings within a few seconds. In a vacuum this period is extended to hours or days depending upon the level of vacuum maintained and the properties of the material. PES is a surface sensitive technique in that most of the electrons detected are ionized from molecules near the surface.

The inelastic mean free path (IMFP) is the average distance an electron travels before it is inelastically scattered i.e. it loses energy and changes its direction of travel. The IMFP varies with the initial kinetic energy of the electron and the structure of the material and can be represented with an exponential decay function representing the probability that an electron will be scattered,

$$P(d)=\exp(-d/\lambda), \quad (13.)$$

where λ is the IMFP for electrons of energy E. As the function decays very quickly, it can be shown that most electrons will come from within the distance of one IMFP. Figure 10, from [30], shows for various metals the mean free path of electrons, λ, plotted against the kinetic energy. As shown in the figure λ varies from ~5 Å to a maximum of ~100 Å. In XPS the most commonly used sources are Mg Kα and Al Kα with energies equal to 1253.6 eV and 1486.6 eV respectively and for those energies λ is less than ~20 Å demonstrating the surface sensitivity of XPS.

For experiments where samples must be removed from the vacuum system a glove box is useful to minimize contamination. For this study measurements were performed under ultra high vacuum at a pressure less than $1x10^{-8}$ mbar. A glove box was used for the dipping experiments to minimize contamination.

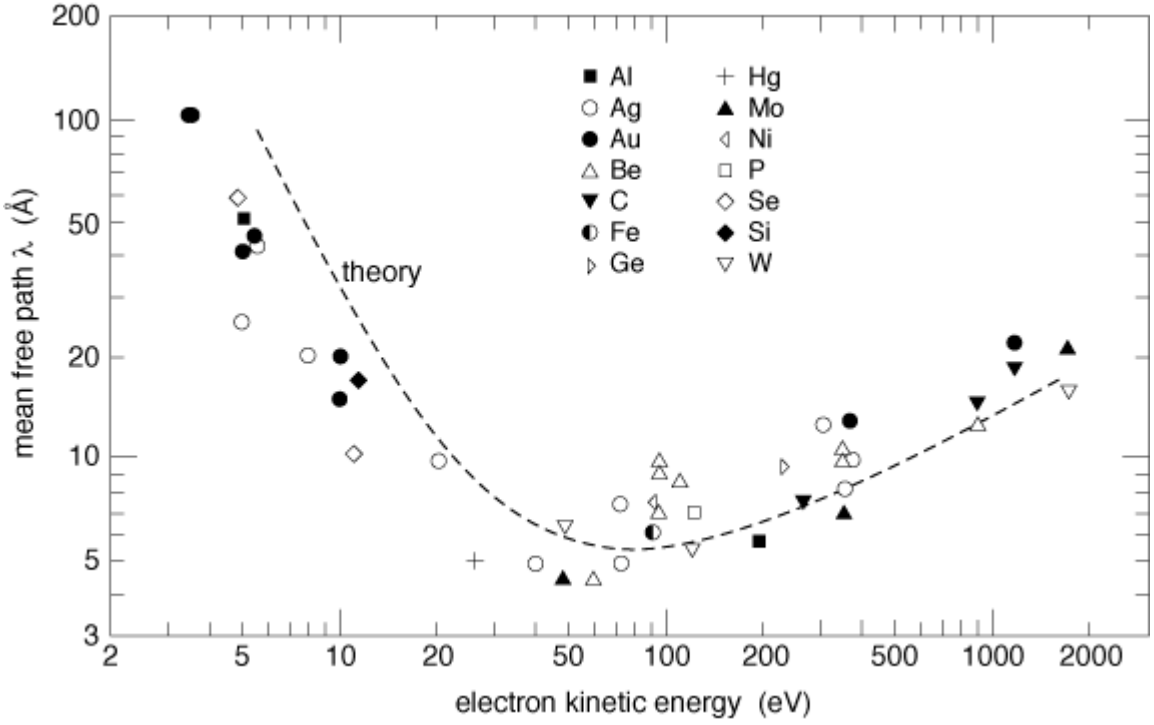

Figure 10: Mean Free Path of Electrons in a Solid

X-ray Photoelectron Spectroscopy

The excitation energy provided by x-rays allows ionization of core electrons from the molecules in sample. For every element in a sample characteristic binding energies can be measured for every orbital in that element. Measuring across the entire range of an x-ray's energy provides a spectrum of the binding energies in a sample. Evaluation of the peaks present in a spectrum will provide information on the elements present in the sample measured. A peak will have a greater intensity if a particular element is present in greater amounts assuming a similar ionization cross section.

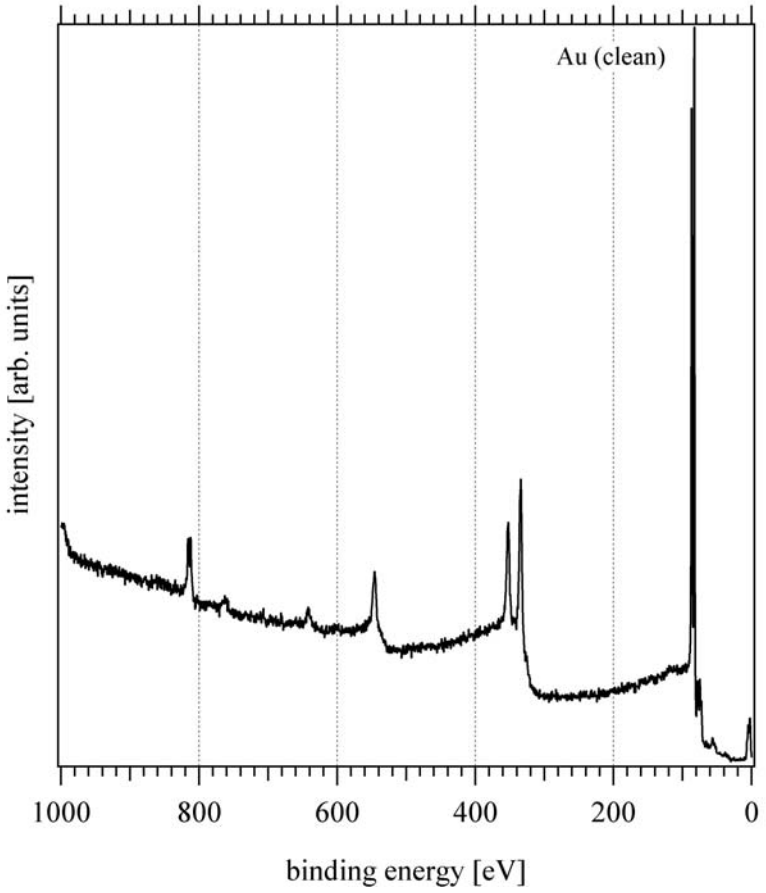

Figure 11: XPS Example, Spectrum of a Clean Gold Sample

A limiting factor on the peaks viewed is the energy of the exciting source. So orbitals with a binding energy greater than the source will not be measured. e.g. The

binding energies of Au's K, L, and M orbitals start at 2206 eV rising to 80,725 eV for the K (1s) orbital. The N and O orbitals are in the range of XPS and represent the spectrum measured via XPS.

Figure 11 shows an x-ray photoemission spectroscopy (XPS) survey measurement of a clean Au sample. The peaks at 5.8 eV, circa 85 eV, 3315 and 353 eV, 546 and 642 eV are all characteristic of Au.

When an electron is emitted from certain orbitals it can create a vacancy in more than one fashion. Each possible configuration will produce a different binding energy result clustered in the same general area. As not all the configurations are equally probable the resulting peaks will not be symmetric nor have equal intensity. The resulting split is always the same characteristic split for each orbital, where it may occur, in an element. One of gold's spin doublets can be seen between 300 and 400 eV in Figure 11.

XPS can reveal information on the chemical and physical states near a sample's surface. These can be noted by the shifting of peaks to higher or lower energies and by changes in relative intensity between two peaks. Figure 12 shows a small shift in an O 1s peak and a small change of intensity between the two peaks. These measurements were taken from L-cysteine evaporated upon Au and exposed to x-rays for an hour (a discussion is in the Results section). The change of intensity indicates a loss of O and the shift to a lower energy indicates the breaking of bonds.

Ultraviolet Photoelectron Spectroscopy

Ultraviolet light provides an excitation energy which will ionize the valence electrons of a sample. The gas discharge lamp typically used for UPS provides a very narrow line width of radiation and a large flux of photons. The narrow line width provides a good resolution and the large flux provides a high signal to noise. The typical energy measured is He I which is 21.2 eV. This level of energy allows investigation of the electronic structure at the surface of a sample. This includes determination of the highest occupied molecular orbital (HOMO) and charge injection barriers. Due to the

low energy a bias voltage is typically used to ensure ejection of electrons from the sample.

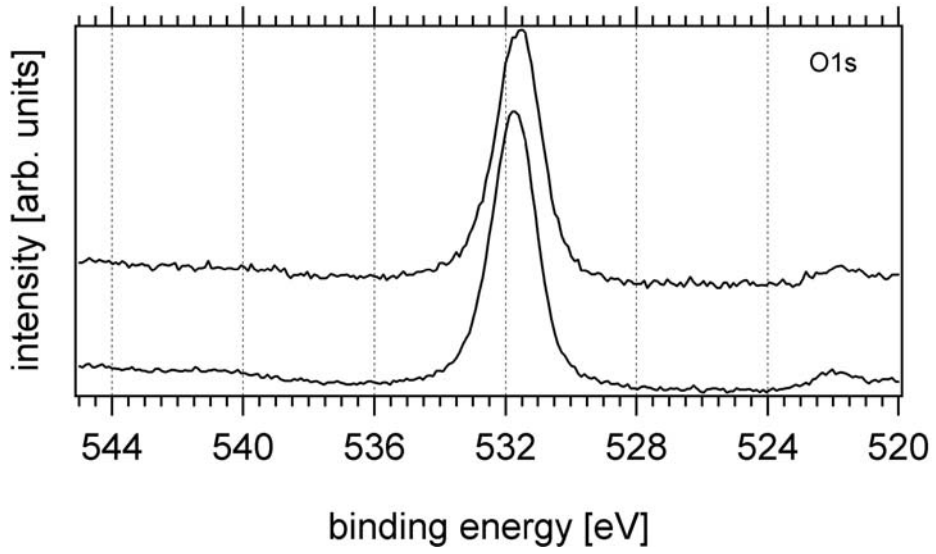

Figure 12: Peak Shift Example, Spectra of Two O 1s Core Level Peaks with the Top Spectrum Shifting After Exposure to X-ray Radiation

Experimental

Three experiments and several supporting and clarifying experiments were conducted to investigate the L-cysteine/Au interface. The primary experiments consisted of two experiments with dipping into solution and one experiment with evaporation. In this section the dipping experiments will be discussed and then the evaporation experiment. Additional experiments will be discussed when relevant to the topic at hand. Prior to discussion of the actual experiments the equipment used and the experimental setups will be covered.

Experimental Method

All measurements were conducted using an ultra high vacuum (UHV) system, shown as a block diagram in Figure 13, consisting of four chambers: a fast entry lock, two preparation chambers, and a measurement chamber. The system is commercially available from SPECS (Berlin, Germany). The base pressure of the system is $1x10^{-10}$ Torr. The analysis chamber is equipped for photoelectron spectroscopy (PES) via either XPS or UPS (SPECS non-monochromated XR 50 dual x-ray gun, SPECS UVS 10/35 ultraviolet source, and a SPECS Phoibos 100 hemispherical Analyzer). It is also equipped for Ar^+ ion sputtering with a SPECS IQE 11/35 ion source. Igor Pro software (Wavemetrics, Inc.) was used for all evaluation, graphing and curve fitting.

For the experiments involving dipping into solution a plexi-glass glove box was fabricated in the lab. This box attached to the fast entry lock. For the experiments involving evaporation a thermal evaporator manufactured in the lab was used. Evaporation rates were measured using a commercially available quartz crystal deposition monitor (Inficon, Syracuse, New York). For all experiments commercially available L-cysteine, 97% pure, from Aldritch (product number 168149-25G) was used. Solutions were prepared using methanol. The Au films were 500nm thick upon Si wafers; the Au was deposited via thermal evaporation.

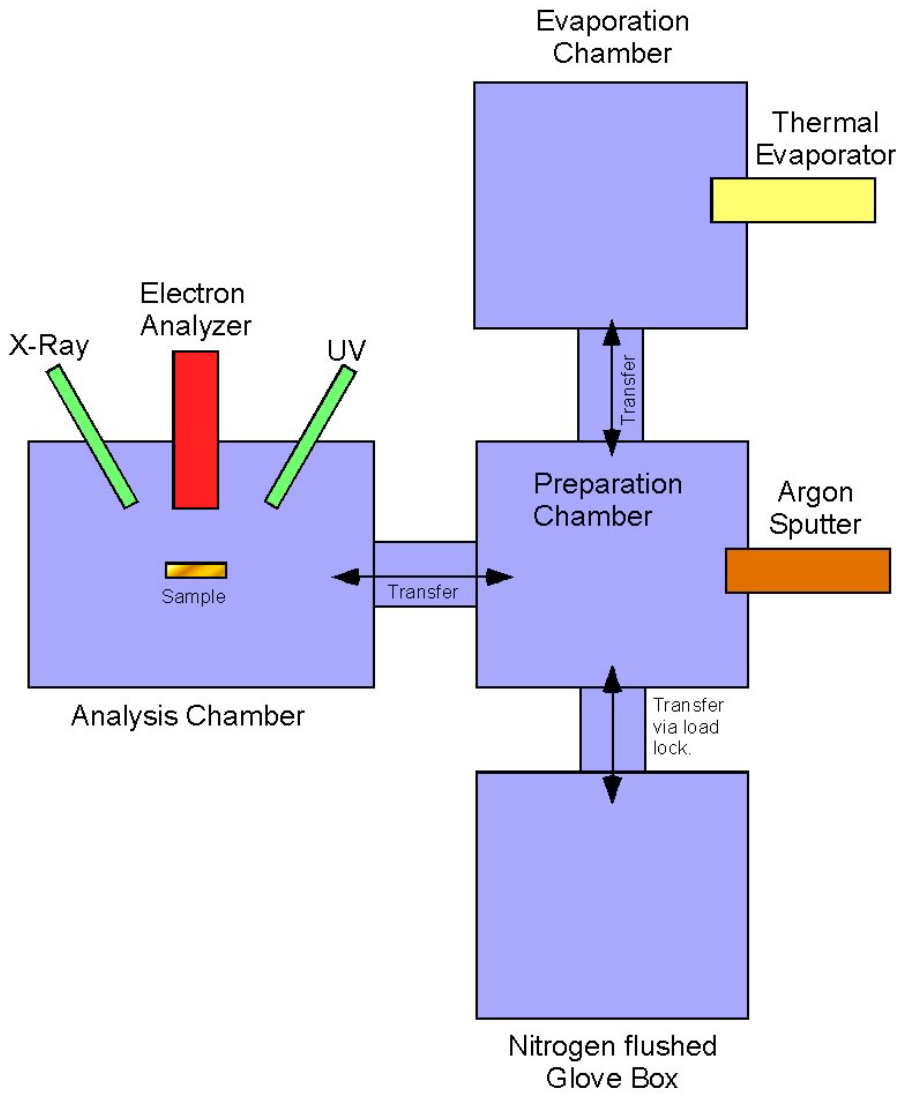

Figure 13: UHV System Block Diagram

A 5 V bias was applied on the sample during UPS He I and XPS work function measurements; the bias allowed separation of sample and analyzer spectral cutoffs. Mg Kα ($h\nu$=1235.6 eV) radiation was used for XPS measurements. Photoelectrons were measured with a SPECS Phoibos 100 hemispherical analyzer.

Gauss-Lorentzian profiles were used when curve fitting in a procedure outlined by Kojima and Kurahashi in [31]. Work function and HOMO cutoff positions were determined by fitting a line into the spectral onsets and using that line to calculate the intersect with the energy axis of the spectra. The resulting values were corrected for analyzer broadening (0.2 eV from the Fermi edge width) by adding 0.1 eV to the fitted cutoff values.

Sample Preparation

This section describes the experimental method for all primary experiments. Methods common to both experiments will be covered then Dipping into solution will be discussed followed by evaporation.

Dipping Experiments

The two dipping experiments were conducted with the same general method. The difference between the experiments was the number of dips, the duration of each dip, and the concentration of the solutions. For this study 9uM (low molarity) and 1mM (high molarity) concentration L-cysteine/methanol solutions were prepared the evening before the experiments. These concentrations were chosen for specific purposes. The high molarity solution was chosen to reflect the concentrations most commonly used in existing papers and the low molarity solution was chosen to slow down the formation of the monolayer in order to make best use of the multi-step deposition method.

The solutions were placed on a magnetic stirrer overnight and used the next day to minimize effects from peptide formation. When placed in the glove box the solutions were covered and were uncovered only for dipping.

Each Au sample was mounted upon a sample holder via silver epoxy to maintain electrical contact during PES. The to be investigated sample, the solution, two stainless steel tweezers, and the sample extractor were placed into the glove box after it had been affixed to the fast entry lock. The tweezers and sample extractor were cleaned with methanol prior to placement in the box.

The glove box was flushed and filled with 99.995% pure N_2 prior to and during experiments. The atmosphere in the glove box was circulated via a diaphragm pump

through filters containing active carbon and Drierite (a dehumidifying agent) in order to remove residual contamination. During experiments a slight overpressure was maintained in the glove box to prevent contamination from the local atmosphere.

The experiments were begun by moving a sample into the preparation chamber and sputtering it at a kinetic energy of 5 keV and an emission current of 10 mA. The Ar pressure was approximately 10^{-5} mbar during the sputtering process. Measurements were then taken via UPS and XPS to demonstrate that a sample was clean and to provide a baseline.

Samples were then moved to the fast entry lock. The lock was vented with N_2 and the sample extracted into the glove box. Each sample was then dipped into the solution for the necessary amount of time. Upon removal from the solution a small amount typically adhered to the bottom of samples. A sample's edge was pressed against a piece of lint-free lab tissue (Kim wipes) to wick away the excess. Samples were then dried by being placed before the fresh nitrogen flow in the box. This evaporated any remaining solvent. Samples were then replaced into the fast entry lock for transfer to the analysis chamber.

In that chamber another set of UPS and XPS measurements were taken. The cycle was then repeated; dip then measure until the appropriate number of steps was completed.

Evaporation Experiment

L-cysteine thin films formed via evaporation have been previously characterized via XPS [15] and in this study such characterization is extended by using UPS and multiple deposition steps to respectively investigate the electronic structure and changes in chemical states as the film is deposited.

The evaporation experiment did not require the glove box as the entire operation took place inside the UHV. A Au sample was mounted via silver epoxy upon a sample holder to maintain electrical contact. The experiment was begun by moving the sample into the preparation chamber and sputtering it at a kinetic energy of 5 keV at an emission current of 10 mA. The Ar pressure was approximately 10^{-5} mbar during the sputtering

process. Measurements were then taken via UPS and XPS to demonstrate that the sample was clean and to provide a baseline.

The sample was then moved to the second preparation chamber. In that chamber the L-cysteine was evaporated at a constant rate of 0.3 Å/s as measured by the crystal monitor. During evaporation the sample was kept away from the source in an adjoining chamber which was open to the evaporation chamber. When the desired rate of evaporation was reached the crystal monitor was retracted, the sample moved into position, turned to face the evaporator for the desired time, turned upright again, and moved into a separate chamber. Subsequent to each step PES measurements were performed.

Results

Dipping Results

For Figure 14 through Figure 17, the spectra of the two experiments are combined. The lower portion of the figures presents the spectra from all steps of the dipping experiment using the 9μM solution, and the upper portion presents the spectra from the 1mM solution experiment. The low molarity solution, 9 μM, shows the slower initial formation and the higher molarity solution shows a very quick formation as the majority of the change usually occurs with the first dip. The time of each dip is shown in seconds along the left side of each graph.

Figure 14 shows the complete XP core level spectra after each dipping step for O 1s. The low molarity dips show an increasing level of L-cysteine being deposited with each step. After the 22s dip the intensity increases noticeably up to the 64s dip in the low molarity solution. Between the last low molarity dip and the second high molarity dip a shift to a lower binding energy occurs. This may be due to a second layer forming upon the initial monolayer.

Figure 15 shows the C1s core level emission lines. Between the 4s and 22s dips a shift is evident in the low molarity spectra. At the top spectra the curve fits are shown relating to the species of carbon found in L-cysteine.

Figure 16 shows the core level spectra for S2p. During the low molarity experiment not S emissions were observed until after the 8s dipping step. This is likely due to the low S content of L-cysteine and the low ionization cross section of that element. At 22s an emission is barely visible and becomes more prominent with the following two steps. In the high molarity sequence the immediate result is plainly visible. In the 80s spectra the two curve fits, at 162.5 and 164.0 eV, representing the two S states are shown.

Figure 17 shows the Au4f core level emissions. A reduction in intensity with increasing dip times is apparent during the low molarity dipping, represents the increasing amounts of L-cysteine being deposited upon the sample surface. In the high molarity portion of the graph, the constant intensity after the first deposition step clearly shows the immediate coverage of the sample.

Figure 18 presents various views of the UP spectra for the high and low molarity dip experiments. The center portion of the graph contains the complete UP spectra obtained during the experiments. On the right is a magnified view of the HOMO portions of the spectra and on the left the is a magnified view of the spectral cutoffs.

The bottom spectrum shows the clean Au sample. The prominent features from 7 eV and below are related to the Au conduction band density of states. The high peaks correspond to the d-bands and the lower slope toward the Fermi edge is related to the the s-p bands. The effects of deposition are clear as the signal from the L-cysteine HOMO overlaps the peaks. Portions of the signal are also reduced in intensity especially on the portion closest to the Fermi edge. In the high molarity experiment the Au signal is almost completely obscured but little change can be observed throughout the entire series.

In the high binding energy cutoff in the low molarity series the major change is a shift from the cutoff of Au at 16.03 eV and the cutoff after the first dip which stabilizes at 16.96 eV. This shift is due to the formation of an interface dipole, eD. As is the pattern for the high molarity experiment the shift is complete in one step without the gradual change seen in the low molarity series.

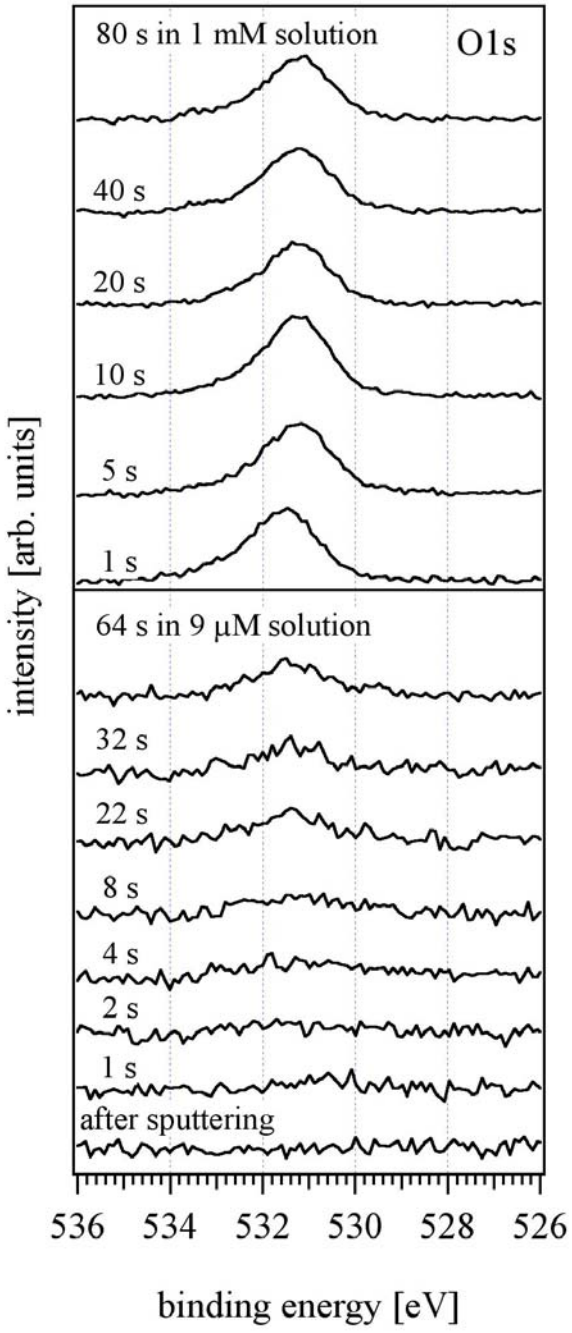

Figure 14: O1s XPS Core Level Spectra for Low (Bottom) and High (Top) Molarity Dips

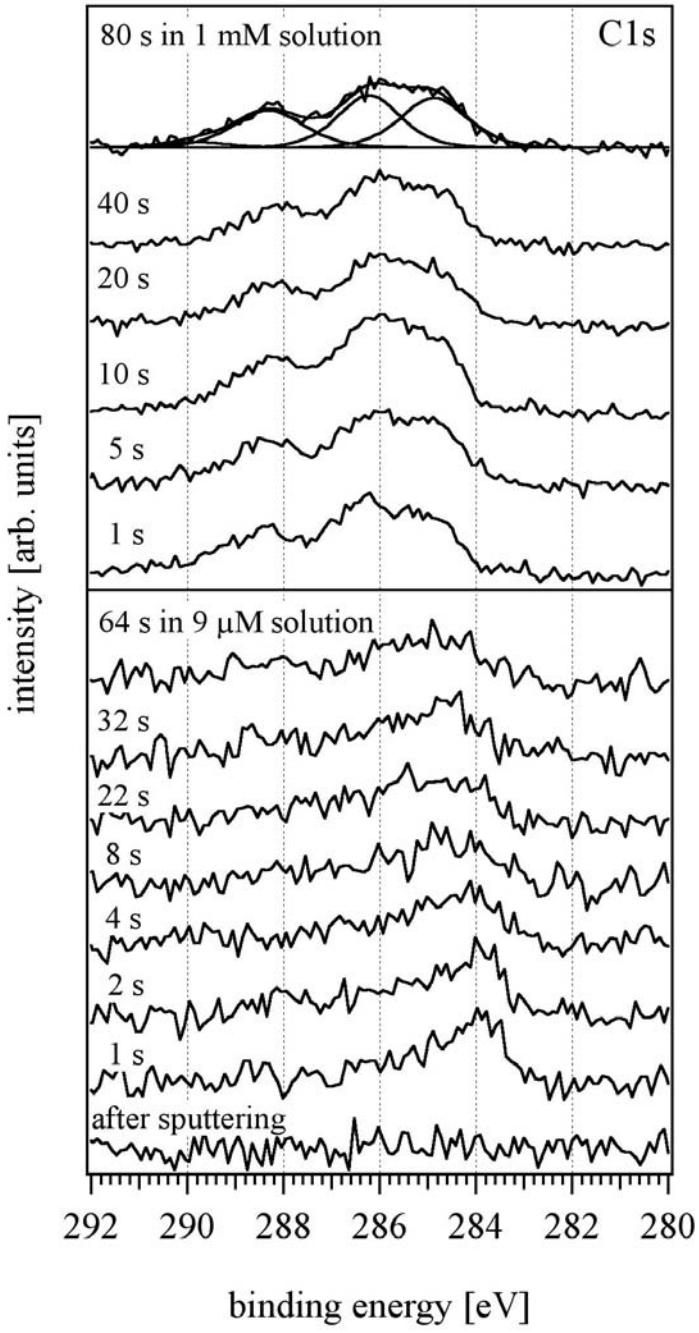

Figure 15: C1s XPS Core Level Spectra for Low (Bottom) and High (Top) Molarity Dips

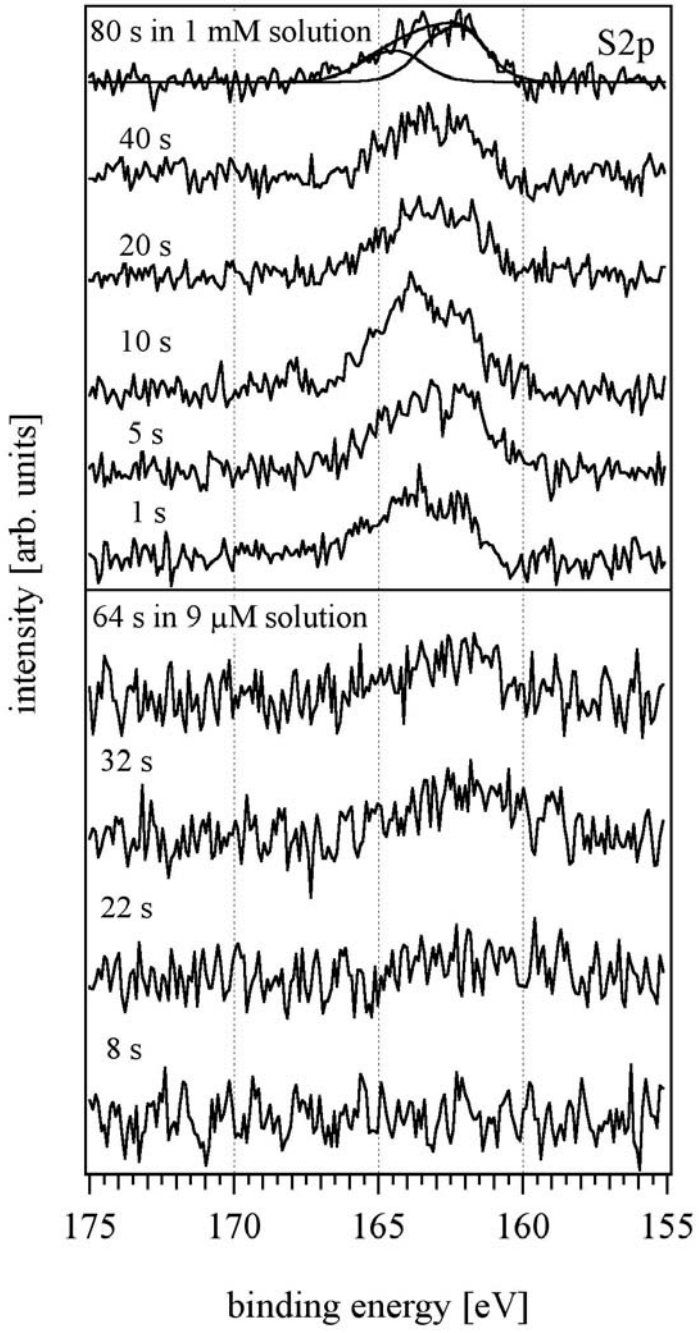

Figure 16: S2p XPS Core Level Spectra for Low (Bottom) and High (Top) Molarity Dips

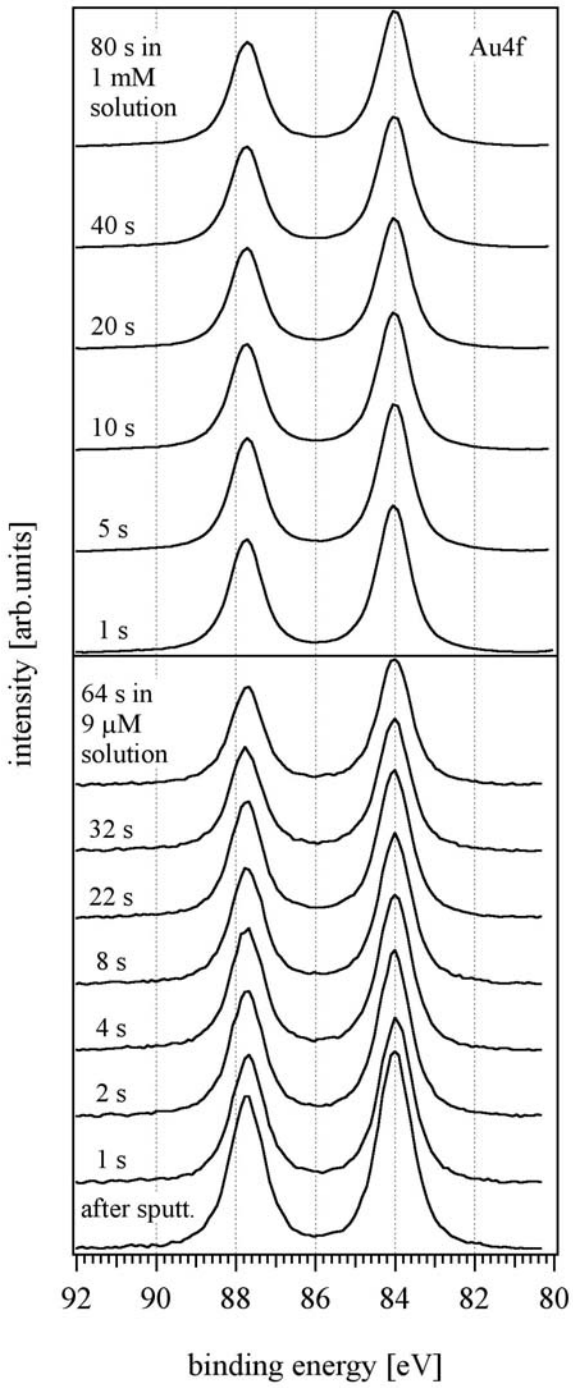

Figure 17: Au4f XPS Core Level Spectra for Low (Bottom) and High (Top) Molarity Dips

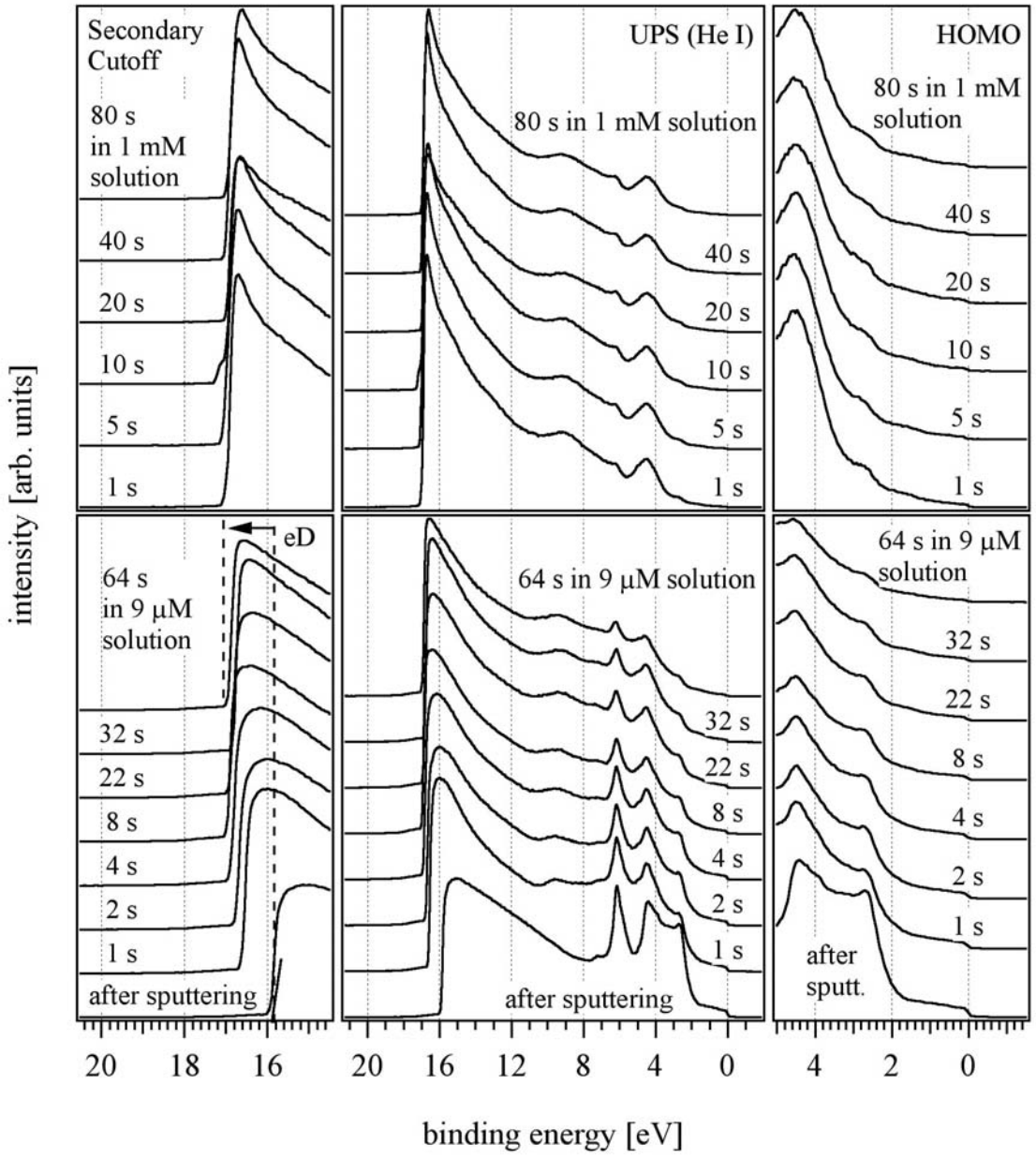

Figure 18: UP Spectra for Low (Bottom) and High (Top) Molarity Dips

Evaporation Results

Figure 19 shows the complete XP core level spectra measured after each deposition step. Figure 20 shows the complete UP spectra measured after each

deposition step, the central portion shows the complete spectra measured after each deposition step. Figure 24 shows a magnified view of each spectrum including the fitted peaks.

The parameters in the figures represent the calculated thickness for that experiment based upon 0.3 Å/s (as determined from the crystal monitor) multiplied by direct exposure time, starting with 3 seconds for the first exposure to 189 seconds for the last exposure.

The Au 4f core level emissions with the characteristic doublet are shown on the far right of Figure 19. After the first two evaporations the intensity of the emissions is not significantly decreased. Starting with the third evaporation, 6.3 Å, the intensity begins to decrease and decreases considerably over the next two spectra before finally disappearing. The last spectrum indicates that the L-cysteine fully covers the surface and that the thickness exceeds the IMFP of the Au 4f electrons.

The center of Figure 19 shows the C1s core level emissions. The spectra are composed of three different carbon species found in L-cysteine. All three emissions are evident after the first evaporation but a significant intensity change is not noted until the fourth evaporation, 13.5 Å.

The far left side of Figure 19 shows the O1s core level emissions. The emissions show two oxygen binding energies at 531.3 eV and 532.2 eV. A significant intensity change is not noted until the fourth evaporation, 13.5 Å, this corresponds to the decrease in the Au4f intensity and increase in the C1s core level emission intensity.

The S2p core level emissions with the characteristic spin doublet are shown to the right of center in Figure 19. The initial evaporations result in a low intensity emission at about 162 eV, this emission is consistent with previous measurements [32] using an Au sample dipped into L-cysteine dissolved in methanol. Starting with 13.5 Å the emissions are dominated by emissions at 164 eV and 165.2 eV.

Left of center in Figure 19 shows the N1s core level emissions. The thinner layers, 0.9 -6.3 Å, show a binding energy of 401.7 eV, starting at 13.5 Å a second peak at 399.6 eV is evident. The energy level 401.7 eV is attributed to the NH_3^+ state found in the amino group and 399.6 eV is attributed to the chemical state of nitrogen in NH_2.

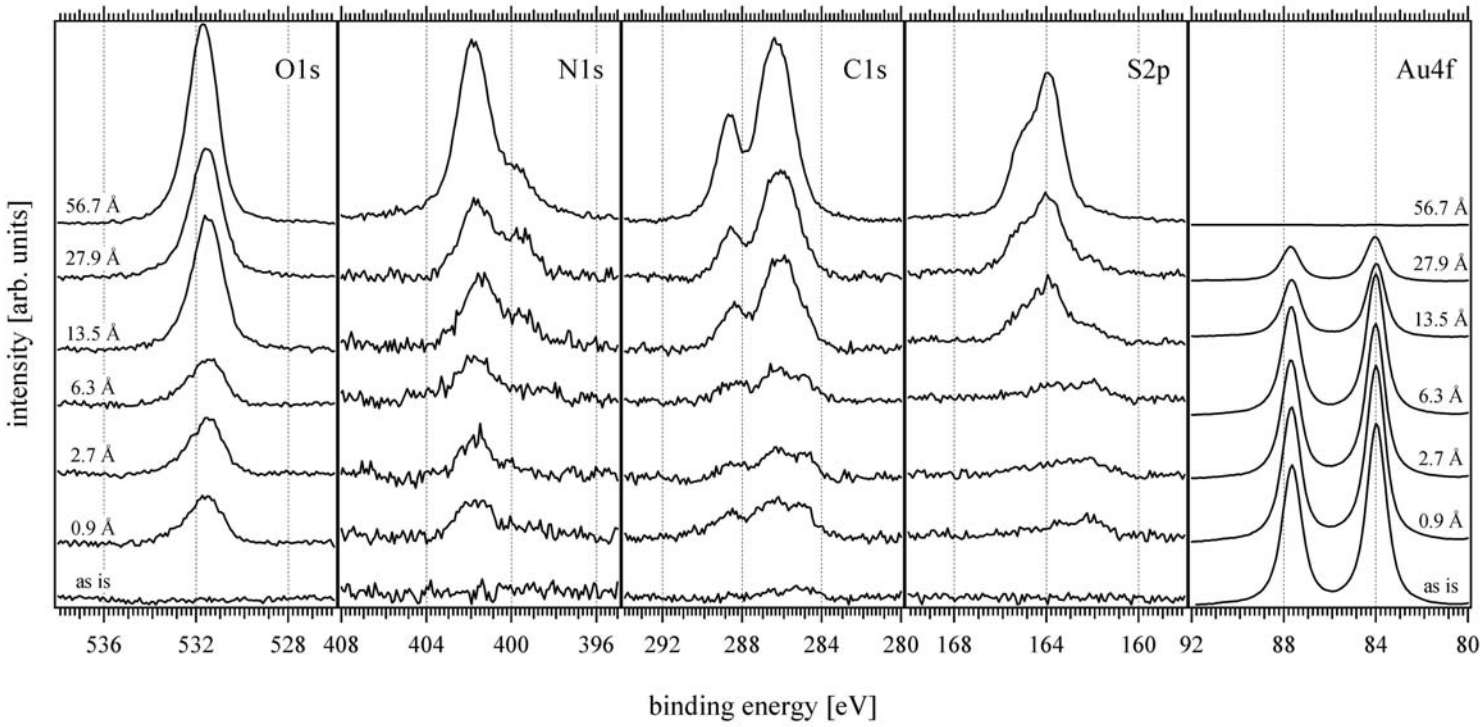

Figure 19: Evaporation of L-cysteine on Au Core Level Spectra for O1s, N1s, C1s, S2p, and Au4f (from Left to Right)

Figure 20 shows the results of the corresponding UPS measurements. The center graph shows the entire spectra as measured during the evaporation series. The high binding energy cutoff is shown on the left and the Au conduction bands/L-cysteine HOMO region is shown on the right. Both are magnified to show detail. The "as is" spectrum is the spectrum of the clean Au surface after Ar^+ sputtering. The Fermi edge is defined as 0 eV. The segment of the spectrum between 0 eV and 7 eV represents the Au conduction band density of states. After the initial evaporation the high binding energy cutoff shifts due to the formation of an interface dipole, eD. The high binding energy cutoff of the "as is" spectra at 15.94 eV corresponds to a work function of 5.28 eV. That cutoff shifts after the initial evaporation due to the formation of an interface dipole, eD, settling at a value of 16.92 eV and a work function of 4.30 eV as shown by the dashed lines on the left side of figure 2. The shift remains constant until 27.9 Å where some broadening occurs and at 56.7 Å where the entire spectrum shifts due to charging with the high binding energy cutoff moving to 17.94 eV.

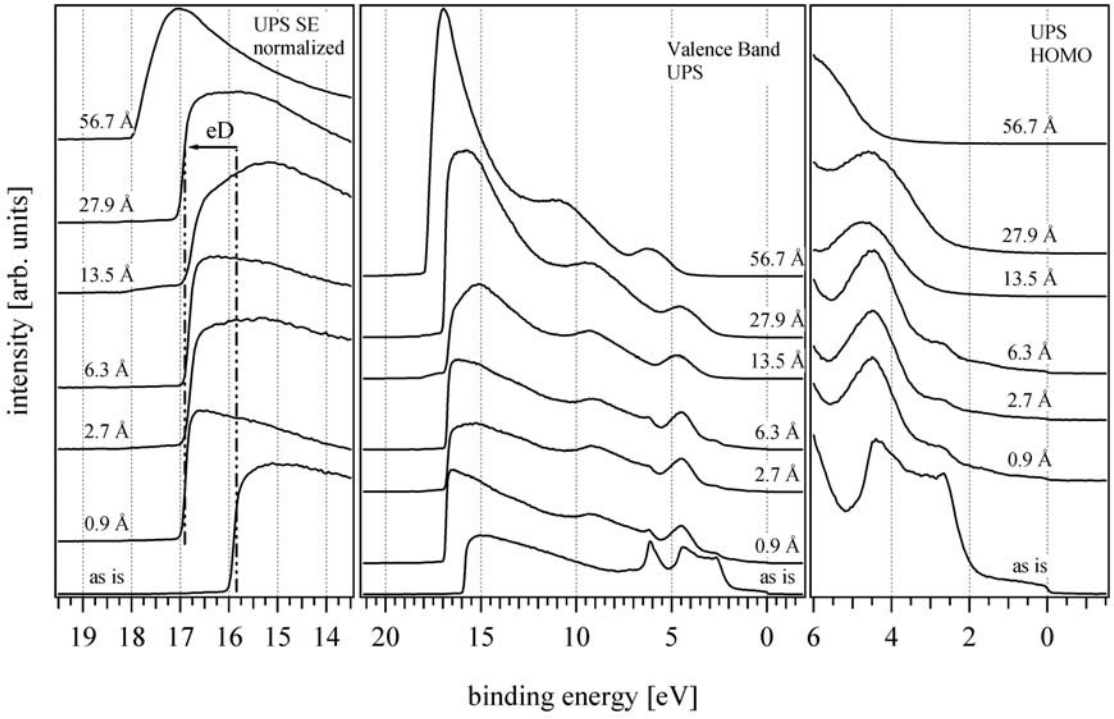

Figure 20: Evaporation of L-cysteine on Au UP Spectra

Discussion

Dipping

Interface Chemistry

Evaluation of the XPS measurements produces results consistent with other published works on the L-cysteine/Au interface [8, 13, 15, 33, 34]. Change in the S binding energy of the thiol, when binding to Au, is a key indicator of the formation of the self-assembled monolayers. In the low molarity dip experiment this can be seen in the spectrum after 32s total dip-time. A less visible peak is also visible through the noise of the 22s total dip time spectrum. This peak is at approximately 162 eV which was previously assigned [15] to chemisorbed L-cysteine which is consistent with the formation of a self-assembled monolayer. In the high molarity sequence two peaks are readily apparent after the 1s dip. One peak is at 162 eV and the other is at 164 eV. The 164 eV peak was also assigned in Ref. [15] as being due to physisorbed bulk L-cysteine molecules located on top of the monolayer.

These results demonstrate that during the low molarity experiment the primary process is chemisorption, where the L-cysteine bonds to the Au through the thiol group. During the high molarity experiment both chemisorption and physisorption processes are apparent. In the high molarity experiment some of the molecules are likely physisorbed on top of the quickly formed SAM, which consists of chemisorbed molecules. The generally constant intensity of the S2p emissions during the high molarity dip demonstrates that both processes have limits. The chemisorption process is physically limited by the Au surface available to it. The physisorption is limited by equilibrium between the physisorbed molecules that are desorbed back into the solution and the molecules which adsorb to form a layer.

Examination of the C 1s low molarity dip spectra shows a shift from the initial energies shown in the 1s and 2s spectra to the final energies shown in the 32s and 64s

spectra. The 64s spectrum is consistent with the energies found in the high molarity sequence

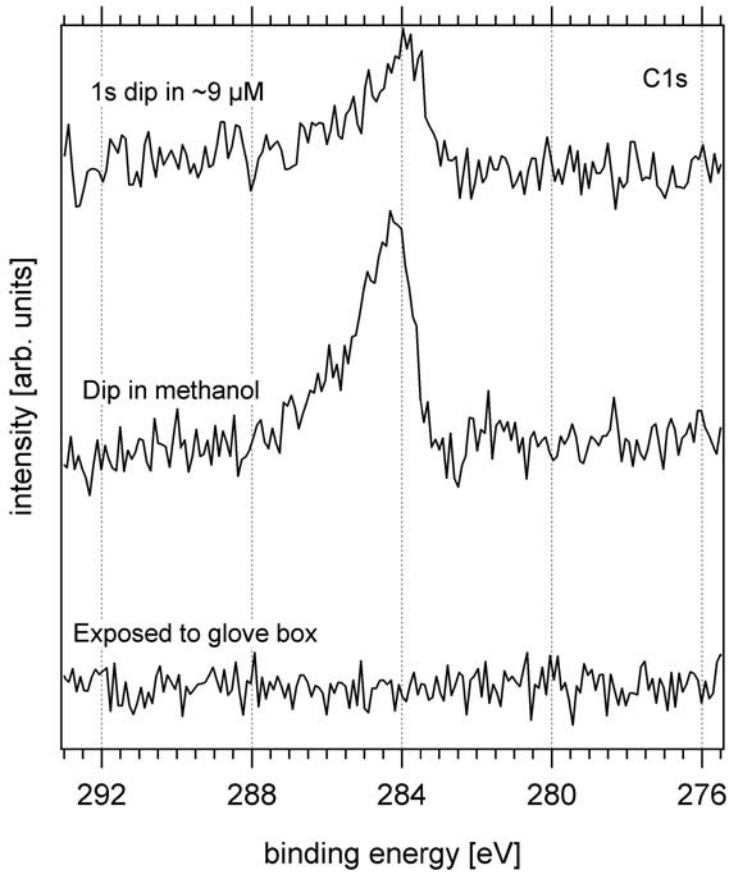

Figure 21: Glove Box Test: from Bottom to Top: Clean Sample Exposed to Glove Box, Clean Sample Dipped in Methanol and 1 s Dip in Low Molarity Solution

An additional experiment in which a clean Au sample was dipped in pure methanol was performed. The results can be seen in Figure 21 and are shown with the initial 1s dip for the low molarity experiment. It is clear that the pure methanol dip and the initial 9 µM dip produce similar results indicating that the initial low molarity C1s emissions are related to chemisorbed methanol. It has been shown in [35, 36] that methanol can be disassociated and adsorbed on Au especially in the presence of OH

which is present in L-cysteine. Hence, the emissions are likely related to adsorbed methanol fragments.

As the L-cysteine bonds to the surface it displaces the methanol and the shift occurs. This is supported by the high molarity experiment where no shift is seen due to the quick coverage of the Au, as the dips progress no change is apparent in the spectra. This also indicates that a complete layer is formed with the first dip and that this does not change with subsequent dips.

As the monolayer forms, the initial methanol fragment emissions are replaced with emissions consistent with L-cysteine bonded to Au. The final low molarity dip presents a spectrum which closely resembles the high molarity spectra. In the 1 mM 80s dip spectra the peak fits are presented showing energies at 288.2 eV, 286.2 eV, and 284.6 eV. The latter energy would normally indicate some form of hydrocarbon, C-C, contamination.

The C binding energies have previously been assigned in Ref. [15]. The highest binding energy of 288.2 eV was assigned to C=O bond from the carboxyl group. The middle component, 286.2 eV is a product of the superposition of C-N and C-S bonded C atoms in the amino and thiol groups. The lowest component, 284.6 eV, was not assigned by Uvdal et al. A peak in that position would normally be attributed to contamination due to hydrocarbon (C-C). They could rule out contamination as the sample preparation was done via evaporation in a vacuum. That energy peak was observed in monolayers but not in thicker bulk layers. Therefore it is likely related to the bonding mechanism where the dissociative bonding of the SH group changes the charge distribution on the C atom which is bonded to it. This produces a more negative charge distribution resulting in a smaller binding energy. Experiments where preparation was done in atmosphere [8, 12, 13]show significantly more intensity at 284.6 eV. In situ evaporate thin films also present similar features as shown in Figure 19's initial spectra and in [15]. The bottom spectrum of Figure 21 shows the emissions from a clean Au sample which was subsequently exposed to the glovebox environment. In performing this experiment the glovebox was set up as if for an experiment with clean tools and a beaker of methanol. As can be see in the spectrum no noticeable contamination was recorded and as the other

portions of the experiment were conducted under UHV conditions no carbon contamination should be present. The experimental results and the control experiment demonstrate that the glove box produces samples free of significant environmental contamination and are comparable to in situ preparation via evaporation.

In the high molarity O 1s spectra, Figure 14, a shift can be seen between the 1s dip peak and the remaining spectra. The peak in the 1s spectrum the peak is at 531.5 eV while in the following spectra the peak is at 531.2 eV. These emission have been assigned [15] to the oxygen bonded carboxyl group. The peak for the low molarity dip aligns below the 531.5 eV peak indicating that energy is likely associated with the chemisorbtion process changing the environment of the adsorbed molecule. The 531.2 eV peaks are likely related to the physisorbed molecules.

The Au 4f peaks do not change their binding energy positions during either of the experiments. During the low molarity dip sequence a reduction of intensity can be seen likely indicating the formation of the monolayer. For the high molarity sequence no change of intensity is noted, indicating the immediate coverage of the sample does not change. For both sequences the FWHM values do not change significantly. An estimate of the final coverage can be made by measuring the final peak intensity and comparing it to the initial intensity. A simple decay function can be used for this purpose:

$$I = I_0 \exp\left(-\frac{d}{\alpha}\right),$$

where I is the measured intensity of the adsorbate covered substrate, I_0 is the initial intensity, d is the thickness of the adsorbate layer, and α is the mean free path of the emitted photoelectrons. Solving the equation for d we can make the estimate. The intensity ratio $I/I_0=0.66$ is found by taking the peak areas from the 80s dip in the high molarity solution and the clean substrate. The mean free path is estimated to be 14Å for electrons of 1402.65 eV kinetic energy (using the 1486.6 eV excitation energy and the 83.95 eV binding energy)[37]. The result is that d = 5.8 Å which represents the final overlayer thickness estimate. The UPS data, Figure 18, supports that estimate as the final dip still shows signs of the Au conduction bands. That thickness also corresponds to the 5Å thickness estimated in Ref. [15] for layers prepared via solution and a 6Å thickness

was estimated for evaporated layers. In that paper, Uvdal et al propose a model where the physisorbed layer partly overlaps the chemisorbed layer similar to the teeth in a zipper.

Electronic Structure

The UP-spectra in Figure 18 can be used to determine the electronic structure of the interface i.e. the interface dipole and the charge injection barrier can be obtained. In the low molarity series at the bottom of the figure the change from pure Au substrate to Au with L-cysteine layer can be observed. In the 64s dip the Au conduction band features are still visible at approximately 6 eV and spread around 4 eV but they are obscured by the L-cysteine HOMO emissions. One difficulty is separating the Au conduction band from the HOMO emissions.

The interface barrier is not difficult to determine as it can be taken directly from the shift in the secondary cutoff as there is no band bending or charging in this case. On the left side of Figure 18 the secondary cutoff is magnified and the interface dipole, eD, is shown. The dipole was determined to be 1.03 eV representing a shift from a lower energy with the Au substrate to a higher energy with the L-cysteine layer present. The direction of the shift indicates that the L-cysteine molecules transfer negative charge to the Au substrate. The dipole is formed at the interface by localized charge transfer as a result of the chemisorption process.

Next the charge injection barrier from the L-cysteine HOMO to the Au Fermi level must be determined. Since the binding energy scale is calibrated to be zero at the Au Fermi level the charge injection barrier can be determined from the L-cysteine HOMO. Fitting a straight line to the HOMO edge to determine the intersection with the binding energy axis provides the desired information. In the case of this experiment the superposition of the Au conduction bands and the L-cysteine HOMO makes this process difficult.

An additional experiment was conducted to assist in this process. 125 Å of L-cysteine were evaporated upon highly oriented pyrolitic graphite (HOPG). The conduction bands of HOPG are very weak as can be seen at the top of Figure 22 where

the background removed UPS spectrum of L-cysteine/HOPG is shown with the clean HOPG conduction bands spectrum for comparison. It demonstrates that no significant superposition is present between the two. It shows HOMO features at about 8.5 eV and 4.2 eV.

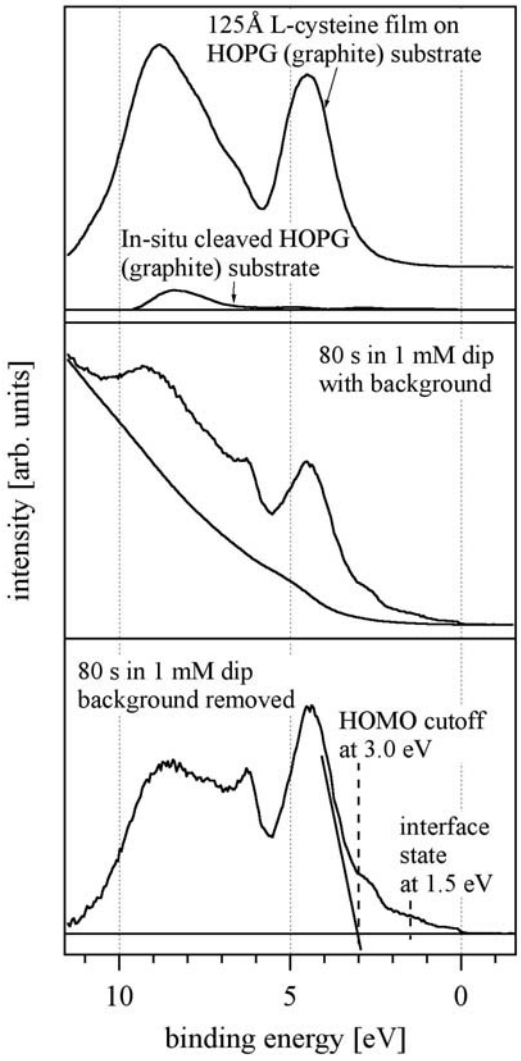

Figure 22: Demonstration of HOMO Cutoff Determination Using HOPG to Determine Location of L-cysteine HOMO Features

In the middle of the figure the 80s dip in the high molarity solution is presented with the background line. The bottom of Figure 22 shows the same spectrum with the background removed. A line fitted to the 4.2 eV peak edge results in an intersection at 2.9 eV. An adjustment for analyzer broadening of 0.1 eV puts the cutoff at 3.0 eV which directly corresponds to the charge injection barrier between the L-cysteine HOMO and the Au Fermi level.

A weak emission feature at 1.5 eV is apparent in the L-cysteine spectra on the bottom of the figure. Comparison with the upper portion of the figure demonstrates that this feature is not present in the L-cysteine spectrum. Figure 22 shows a magnification of that portion of the binding energy scale. From top to bottom the figure presents a sputtered clean Au surface, the low molarity 64s dip, the high molarity 80s dip, and L-cysteine on HOPG. The weak feature is not present in either the HOPG or the clean Au spectrum which suggests it may be due to the process of chemisorption between Au and L-cysteine. This feature may represent an interface state gap in the L-cysteine HOMO/LUMO (lowest unoccupied molecular orbital) gap induced by the interaction with the interface. The interface state may act as a stepping stone for charge transfer between L-cysteine and Au.

The electronic structure is summarized in Figure 28, a schematic of the orbital lineup between L-cysteine and Au. In the center it can be seen that both energy levels are pinned at the Fermi level, E_F. At the top the interface dipole, eD, shows the barrier between the vacuum levels from Au to L-cysteine. At the center bottom the L-cysteine HOMO is shown as 3.0 eV and to the right the level of the interface state is shown at 1.5 eV. The work function of Au is determined to be 5.28 eV which agrees with previous results [38]. Subtracting the 1.03 eV interface dipole from the Au WF puts the L-cysteine work function at 4.25 eV. Adding that result to the charge injection barrier (in this case the HOMO) produces an ionization energy of 7.25 eV for the bonded L-cysteine layer. If the HOMO-LUMO gap were known, the charge injection barrier between the LUMO and the Au-Fermi level could be determined. A theoretical study, [9],of the cysteine/Au interface placed the LUMO at 4 eV above the HOMO [15], which would put it just 0.25 eV below the vacuum level, E_{vac}.

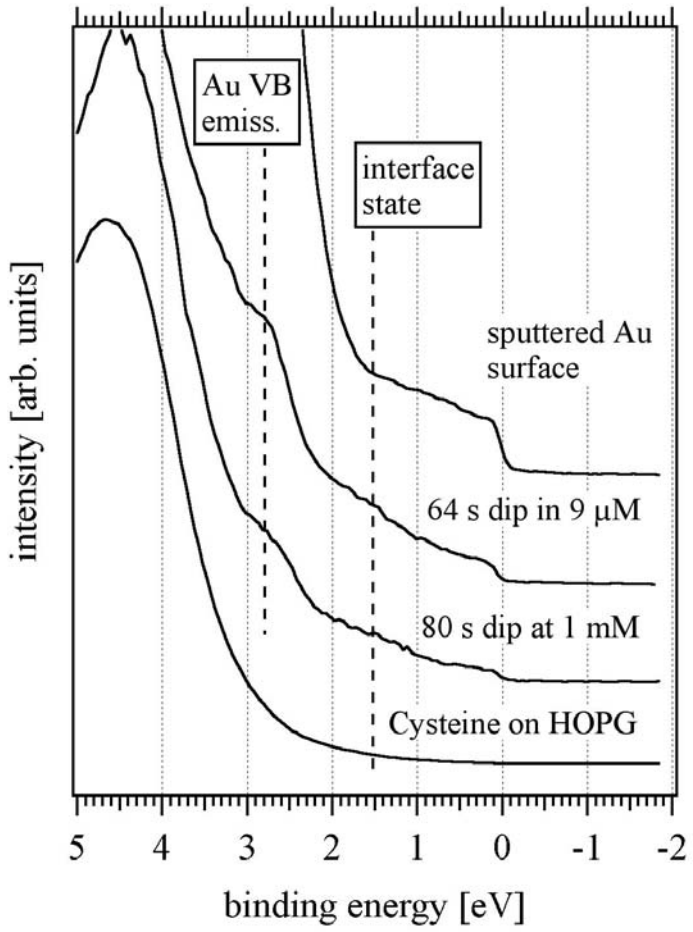

Figure 23: Comparison of L-cysteine on HOPG and on Au Near HOMO Cutoff. Note Interface State at ~ 1.5 eV

Evaporation

Interface Chemistry

Evaluation of the XPS measurements produced results consistent with other published works on the L-cysteine/Au interface [8, 13, 15, 33, 34]. The S2p spectra are most indicative of these results; in the 0.9 Å to 6.3 Å depositions, the resulting binding energies are consistent with the dissociative chemisorption [15] of L-cysteine via its thiol group. After the first evaporation a small peak can be seen at approximately 162 eV, the

intensity of this peak is fairly consistent over the following two depositions. Starting with the fourth deposition of 13.5 Å a peak appears at approximately 164 eV. These emission lines have been previously assigned [15] to chemisorbed L-cysteine species (162 eV) and bulk L-cysteine molecules physisorbed on the self assembled bonded layer (164 eV). This data indicates that during the initial evaporations the L-cysteine mostly binds to the Au via its thiol group and during later evaporations is adsorbed on top of that layer.

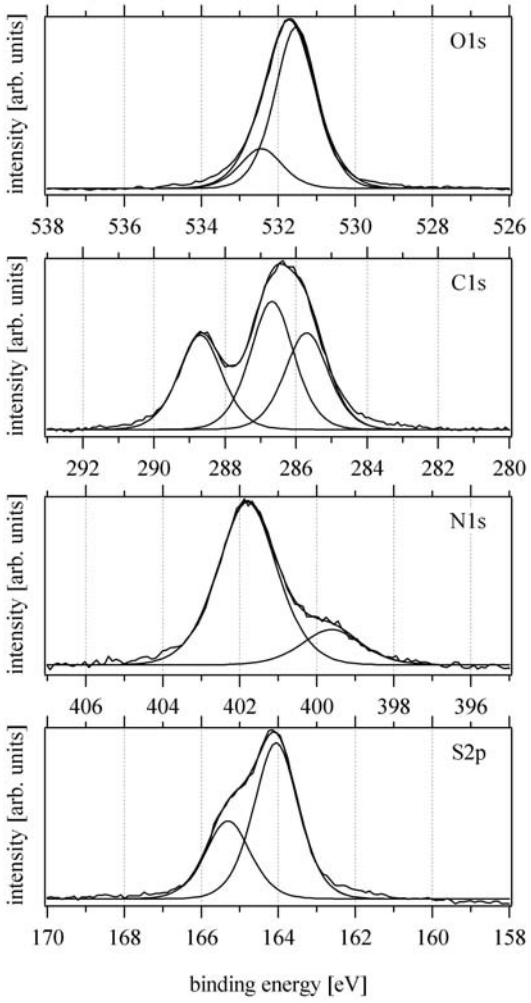

Figure 24: Final Evaporation of L-cysteine of Au Spectra with Curve Fits

The C 1s 56.7 Å core level spectrum was fitted with peaks at 285.6 eV, 286.6 eV, and 288.6 eV, Figure 24. As the UPS spectrum for that evaporation shows some charging a fit was also completed on the 6.3 Å which was fitted with peaks at 284.8 eV, 286.4 eV, and 288.4 eV as shown in Figure 25. These have been assigned previously [13, 15] to the C-C; C-N, C-S, and C-OH; and C=O states respectively. The presence of hydrocarbons (the C-C bonds) is typically indicative of contamination. As this experiment was carried out in ultra high vacuum on a sample shown to be clean after sputtering contamination related emissions can be ruled out. Reduction of the 288.6 eV peak due to x-ray damage is not visible in the spectra as it takes approximately 3 hours of x-ray exposure to be readily apparent and a new layer was evaporated after each hour of exposure.

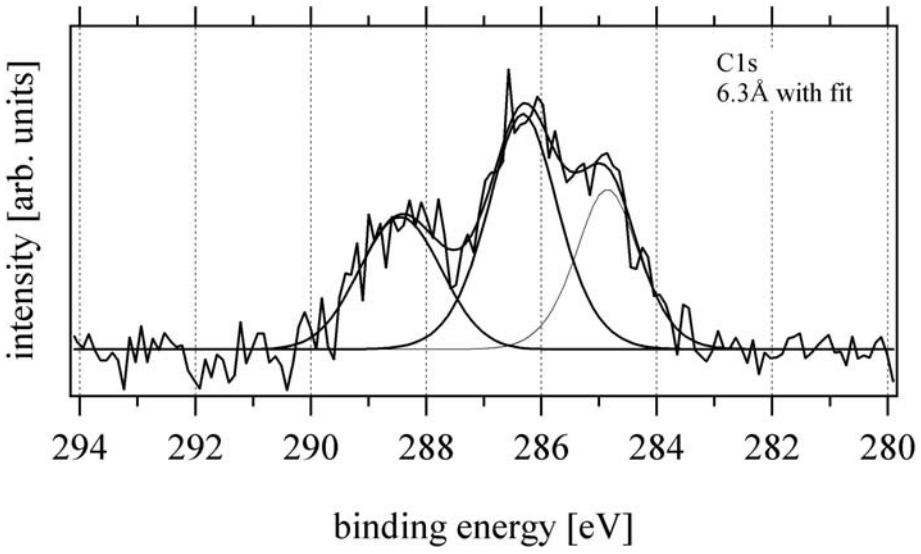

Figure 25: 6.3 Å Evaporation of L-cysteine on Au Fit

The N 1s core level spectra were fitted with peaks at 399.6 eV and 401.7 eV. These energy levels correspond with the values found by Dodero et al in [13], who placed Au substrates into L-cysteine solution. At the 6.3 Å evaporation,Figure 19 ,the 399.6 eV component (NH_2) is visible and becomes more prominent after the 13.5 Å deposition. The 399.6 eV peak is consistent with x-ray damage of L-cysteine as shown by [39] and

our own results. For the last two depositions the intensity does not change significantly while the 401.7 eV (NH_3^+) component greatly increases due to a much greater thickness of L-cysteine being exposed to the same amount of energy.

The change in relative intensity of the O 1s components should be noted as after the first three evaporations the intensity of the 531.3 eV peak increases very quickly compared to the 532.2 eV peak. 531.3 eV is consistent with oxygen in bulk L-cysteine. The 532.2 eV energy was noted during dipping experiments [32], and was proposed to be related to the change in the chemical environment of the molecule in the dual layer structure, such as interaction with NH_3^+ in a dual layer structure. This is supported by the small change in the intensity of that peak as the adsorbed L-cysteine is entirely covered by a second layer of bulk L-cysteine.

Stoichiometry

The L-cysteine molecule contains 7 H, 3 C, 2 O, 1 N, and 1 S –note that PES cannot detect H. The atomic ratios of the elements making up the molecule should be reflected in the relative intensities of the peaks measured with XPS. The area under each peak, after some calculation, can be used to approximate these ratios.

In this experiment the damage to the L-cysteine layer due to x-ray and UV exposure may complicate evaluation of the stoichiometry. As shown in [39] the SH group is the most stable element in L-cysteine followed by the NH_2 and COOH groups and with the OH group being the least stable. Oxygen is expected to be present in a smaller ratio than normal as it is in two of the least stable groups.

The following relationship was used in the analysis of the integrated peak areas of the O 1s, N 1s, C 1s, and S 2p lines. The formula adjusts the measured areas, A, with ionization cross section, CS; analyzer transmission function, TF; and mean free path of the emitted electrons, MFP. The final result is an absolute intensity, $I_{absolute}$.

$$I_{absolute} = \frac{A}{(CS \cdot TF \cdot MFP)}$$

CS values calculated by Scofield [40] were used. The TF was approximated with the relationship

$$TF = (sqrt(E_{kin}))^{-1},$$

where E_{kin} is the kinetic energy of the emitted electrons. Kinetic energy dependent MFP values were linearly interpolated from the values tabulated by Tilinin et al [41].

Relevant values used in the calculation of $I_{absolute}$ are tabulated in Table 1. The calculated $I_{absolute}$ values were normalized to N 1s furthest right column so that the intensity of $I_{absolute}$(N 1s)=1.

The ratios of C:N, N:S, and C:S are all within the expected stoichiometries of L-cysteine: 3:1, 1:1, and 3:1 respectively. O presents the only aberration as it is present in 1.6:1 where stoichiometry would indicate 2:1. This is likely due to damage on the final layers from x-ray and UV exposure as previously discussed.

Table 1: Stoichiometriy Via Intensity

	Peak area (A)	Crossection (CS)	Mean free path (MFP)	Kinetic energy (Ekin)	Transmission factor (TF)	Absolute intensity (Iabsolute) Normalized to N
N 1s	8222	1.8	23.8 Å	852 eV	0.034	1.0
O 1s	20676	2.93	21.1 Å	722 eV	0.037	1.6
S 2p	8174	1.68	28.8Å	1089 eV	0.030	1.0
C 1s	14640	1.0	26.3 Å	967 eV	0.032	3.1

Electronic Structure

The electronic structure of the interface can be determined from the UP-spectra shown in Figure 20. Evaluation of the L-cysteine/Au interface electronic structure involves determination of the charge injection barrier from the L-cysteine HOMO to Au Fermi level and the interface dipole due to localized charge transfer at the interface due to

the chemisorption process. The process is functionally identical to that discussed in the Dipping Results section.

Up to the 6.3 Å deposition Au related emissions at about 6 eV and 2.8 eV are superimposed to the L-cysteine HOMO emissions. In the 13.5 Å and 27.9 Å depositions the feature at 6 eV is no longer visible. In the 56.7 Å deposition the entire spectrum has shifted due to charging effects, taking that shift into account the Au feature formerly at 2.8 eV is barely visible.

Determination of the charge injection barrier can be performed by identifying the HOMO cutoff position on the ultraviolet photoelectron (UP)-spectra. The bottom graph in Figure 26 shows the determination of the HOMO cutoff on the background removed UPS spectrum. The center graph shows the 6.3 Å evaporation spectrum with the calculated background signal. The background was determined by fitting the integral of the spectrum to the inelastic background tail of the UP-spectrum [42]. The 6.3 Å layer was chosen as it shows the Fermi level, however the HOMO value reflects values found on the 0.9 through 27.5 Å UP spectra.

Using an experiment with HOPG it was previously demonstrated where the L-cysteine HOMO cut off occurs on the binding energy scale. Using the 4.5 eV peak in the 6.3 Å spectrum to fit a line for the cutoff value provides a cutoff position at 3.0 eV. Adding 0.1 eV for analyzer broadening gives a final value of 3.1 eV which corresponds to the charge injection barrier between the L-cysteine HOMO and the Au Fermi level.

The HOMO should not be significantly affected by x-ray damage of the L-cysteine molecule. The HOMO is localized upon the S atom as shown in [9, 10]; [39] demonstrates that the SH group is the most stable of the L-cysteine groups when exposed to x-ray radiation.

Evaluation of the interface dipole can be done by measuring the shift in the high binding energy cutoff or secondary cutoff. The cutoff is magnified in the left hand graph of Figure 20. The shift directly corresponds to the change in the work function due to deposition of the L-cysteine. Using the cutoffs from the “as is” and 0.9 Å spectra, the interface dipole between the Au substrate and the L-cysteine layer was found to be 0.98 eV

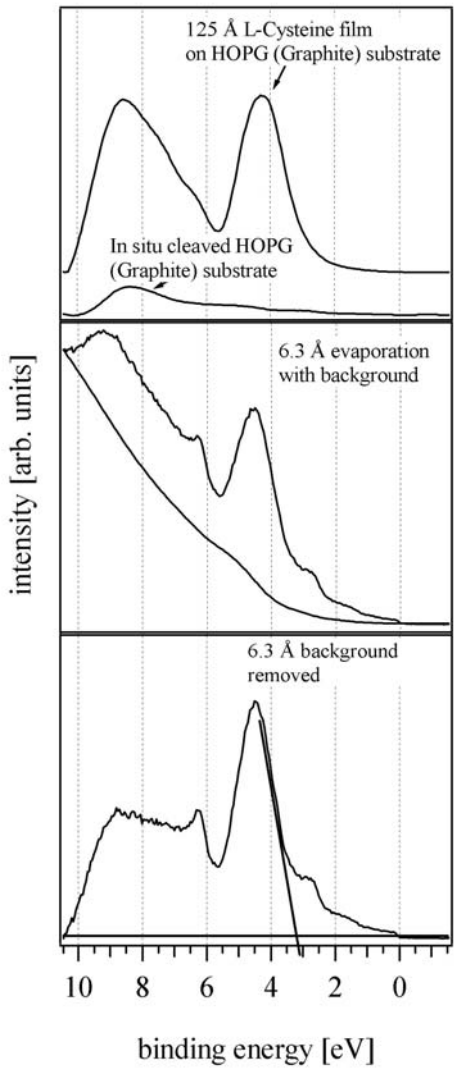

Figure 26: Demonstration of HOMO Cutoff Determination for Evaporation of L-cysteine on Au Using HOPG to Determine Location of L-cysteine HOMO Features

Figure 27 shows a magnified view of four UP spectra which from top to bottom are the sputtered Au surface, the 13.5 Å layer on Au, the 6.3 Å layer on Au, and the 125 Å layer on HOPG. Careful examination of the 6.3 Å evaporation line shows a feature at approximately 1.5 eV which is not evident in any of the other spectra in the figure.

Examination of the UP spectra (fig. 2) shows that the state is also visible on the 0.9 Å and 2.7 Å evaporations. Starting with the evaporation of 13.5 Å that state is no longer visible in the UP spectra. This weak peak is not visible in the HOPG evaporation or in the sputtered Au spectra indicating that it may be related to the formation of the L-cysteine/Au interface. The previous assignment of this emission to an interface state is supported by disappearance of this emission as the overlay increases in thickness.

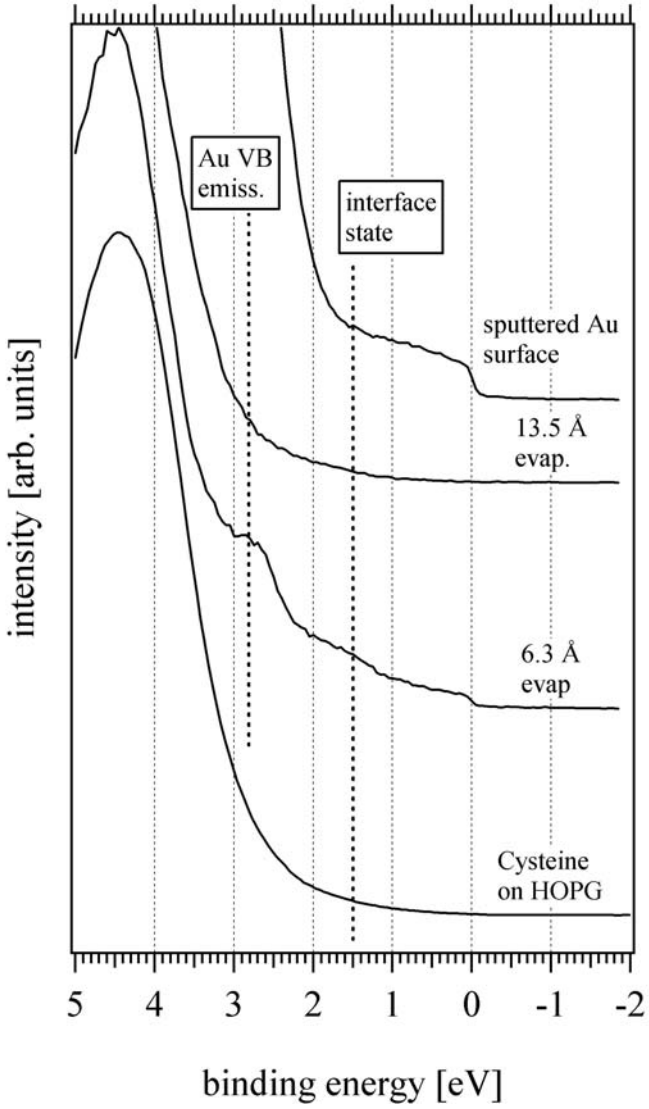

Figure 27: Magnified Portions of the UP Spectra Note Interface State at ~1.5 eV

Figure 28 summarizes the results of the electronic structure by schematically representing the orbital line up between the L-cysteine and the Au substrate. The HOMO cutoff is located at 3.1 eV below the Femi level (EF) of the Au substrate and the Au work function was determined to be 5.28 eV which is in agreement with previous results. The interface dipole, eD, was found to be 0.98 eV which places the work function of the L-cysteine layer at 4.30 eV. The L-cysteine work function and the charge injection barrier total to 7.40 eV which is the ionization energy, E_{ion}, for the bonded L-cysteine layer.

X-ray Damage

In evaluating these measurements it is important to account for damage caused by x-ray exposure. A recent paper [39] examined the effects of exposing amino acids, including L-cysteine, to x-rays for long periods up to 6 hours. Zubavichus et al found that the exposure degrades the L-cysteine with some effects via mass spectroscopy after a few minutes of exposure and effects visible in XPS spectra after about 60 minutes. In order to examine the damage caused during our measurements additional experiments were performed. A Au sample was covered with a thick layer of evaporated L-cysteine and exposed to x-ray radiation from the dual x-ray gun for 6 hours. Every hour a measurement was taken; these xps measurements were <9 minutes. Note that these measurements were taken quickly with few rescans, so the noise is more pronounced than in the previous figures.

Comparison of the results to [39] shows similar features such as the broadening of the N 1s peak due to an additional feature at approximately 399.6 eV, the NH_2 feature noted above, and reduction in the 288.6 eV feature of the C 1s core level spectrum. Also apparent is the reduction in intensity for both O 1s and S 2p (Figure 29). As the S2p is removed a smaller peak at approximately 162 eV this value has been assigned to an S thiol bonded to Au that result is not seen in Zubavichus et al as they used indium and ground cysteine. At the same time the Au peak intensity increases, an indication of the removal of L-cysteine components from the surface and consistent with the findings of Zubavichus et al. This also supports the proposal that L-cysteine bonds to Au via its thiol and then adsorbs upon the bonded material.

The x-ray damage is less of a problem with the dipping experiments as the subsequent dips allowed replacement of damaged molecules via solvation into the solution. Damage features such as reduction in O 1s and S 2p intensity are not recorded.

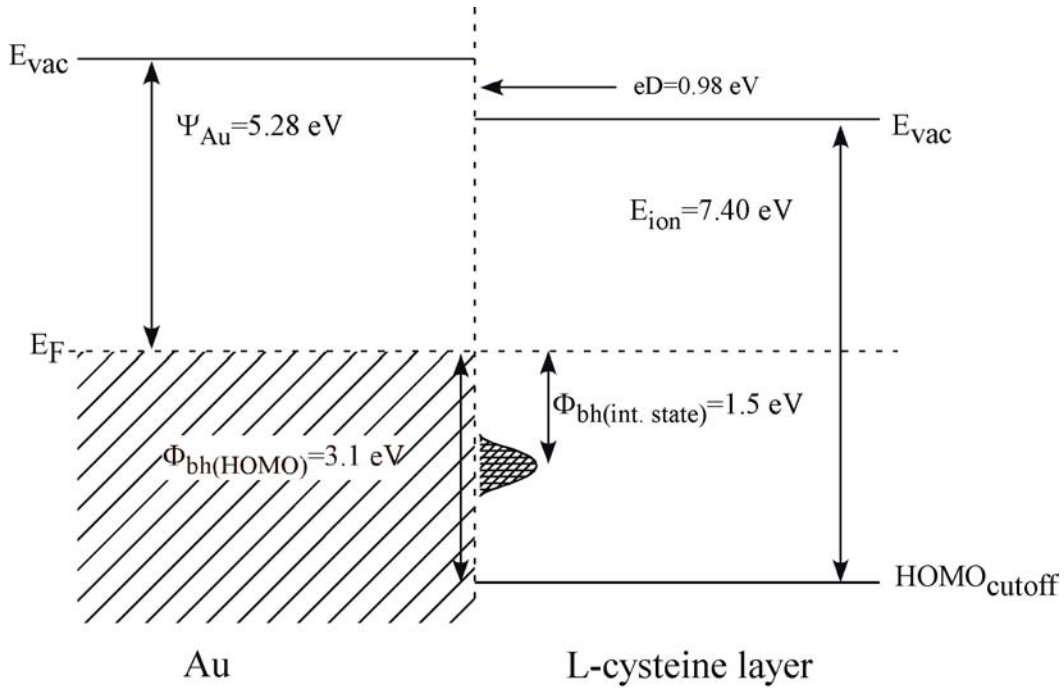

Figure 28: Diagram of the Electronic Structure of the L-cysteine/Au Interface

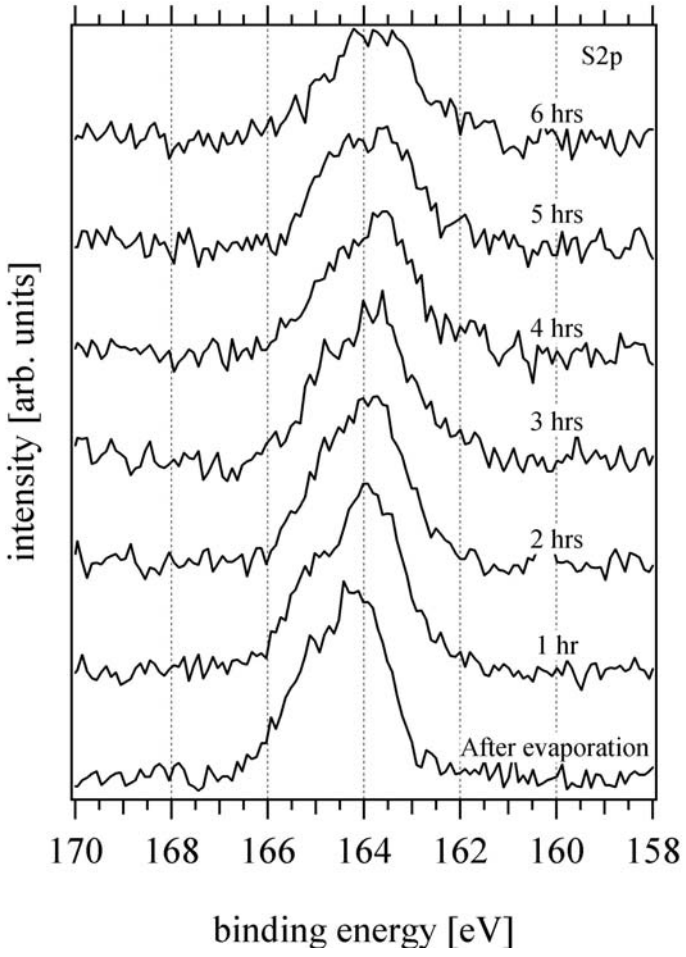

Figure 29: S2p Results from Damage to L-cysteine on Au X-ray Exposure Experiment

Conclusions

Dipping

In this pair of experiments L-cysteine was deposited onto a clean Au surface via dipping into methanol/L-cysteine solutions. The solutions were a low molarity, 9 μM, solution and a high molarity, 1 mM solution with seven and six respectively dipping steps performed. The dips were carried out in a glove box which maintained an environment clean of significant environmental contamination. Measurements were carried out in ultra high vacuum (UHV). X-ray photoemission spectroscopy was performed between each step, and evaluation demonstrated that the results closely agree with previous work [8, 12, 13, 15] on L-cysteine self assembled monolayers on Au substrates. Ultraviolet photoemission spectroscopy (UPS) yielded a charge injection barrier of 3 eV between the L-cysteine HOMO and the Au Fermi level. UPS also allowed determination of the interface dipole, 1.03 eV.

Evidence of an interface state caused by the interaction of L-cysteine and Au was found at approximately 1.5 eV.

Evaporation

In this experiment L-cysteine was evaporated onto a clean Au surface. The evaporation was accomplished in six steps with PES (XPS and UPS) measurements between each step. The XPS results agree with previous work on evaporated L-cysteine/Au interfaces [15]. Additional experiments were performed to determine potential damage produced by XPS. The experiment demonstrated that the damage was similar to the previous work except for the S2p spectra. This was likely due to the difference in methods and the S/Au bonds.

UPS allowed the electronic structure to be evaluated. The charge injection barrier between the L-cysteine HOMO and the Au Fermi level was found to be 3.1 eV, and the interface dipole between the Au substrate and the L-cysteine layer was found to be 0.94

eV. An interface state caused by the chemical interaction between the L-cysteine molecules and the Au substrate was indicated by the measurements at approximately 1.5 eV.

Comparison Between Dipping and Evaporation Experiments

This study produced new results regarding L-cysteine SAMs on Au substrates. New to the body of work are the UPS measurements themselves and the resulting information on the electronic structure, such as the interface state, the L-cysteine HOMO, and the charge injection barrier from the HOMO to the Au Fermi level.

The results for the dipping and evaporation experiments agree substantially. The primary differences lies in the x-ray damage and the electronic structure. The dipping results do not present a noticeable amount of x-ray damage; this is likely due to resolvation of damaged molecules which are then replaced with whole molecules. Evaporation does not offer this replacement mechanism so the damage becomes more obvious with each measurement. The differences in electronic structure are small 0.05 for the interface dipole and 0.1 for the charge injection barrier from L-cysteine to Au. The differences could be due to differences in deposition method and in amount of x-ray damage.

Both the dipping and evaporation experiments resulted in the formation of a possible interface state at approximately 1.5 eV. Further work would be required to better determine the location of the state. These experiments could potentially use a dipping process with a solution that has a molarity between those of the solutions used in this study. It would provide the benefit of producing a more complete monolayer faster than the low molarity solution, and hopefully provide an intermediate step, which the high molarity solution does not quite provide. This may allow the interface state to be more effectively isolated. Angle resolved UPS (or other methods) may also assist in determination of the physical location of the interface state. A recent high resolution XPS study [43] using synchrotron radiation has demonstrated that the physisorbed layer can be removed by heating the system to 100° C. So heating of the sample to provide such a result may assist in such experiments. It would also be interesting to repeat some

of the dipping experiments in this study and to use heating to perform UPS on only the bonded molecules. Such work may yield information on the electronic structure of those bonded molecules and assist in evaluation of the overall interface.

References

1. Rickert, J., A. Brecht, and W. Gopel, Biosens. Bioelectron., 12(7): p. 567-575. (1997.)
2. Verma, N. and M. Singh, Biometals, 18(2): p. 121-129. (2005.)
3. Turner, A.P.F., Science, 290(5495): p. 1315-1317. (2000.)
4. Yu, Q.M., S.F. Chen, A.D. Taylor, et al., Sens. Actuator B-Chem., 107(1): p. 193-201. (2005.)
5. Halko, D.J. and B. Halko, *Treatment of an Orifice Plate with Self-Assembled Monolayers*. 2000, Hewlett Packard Company.
6. Hu, Y., A. Das, M.H. Hecht, and G. Scoles, Langmuir, 21(20): p. 9103-9109. (2005.)
7. Yagi, S., A. Matano, G. Kutluk, et al., Surface Science, 482: p. 73-76. (2001.)
8. Cavalleri, O., L. Oliveri, A. Daccà, et al., Applied Surface Science, 175-176: p. 357. (2001.)
9. Di Felice, R., A. Selloni, and E. Molinari, Journal of Physical Chemistry B, 107(5): p. 1151-1156. (2003.)
10. Di Felice, R. and A. Selloni, Journal of Chemical Physics, 120(10): p. 4906-4914. (2004.)
11. Cavalleri, O., G. Gonella, S. Terreni, et al., J. Phys.-Condes. Matter, 16(26): p. S2477-S2482. (2004.)
12. Cavalleri, O., G. Gonella, S. Terreni, et al., Phys. Chem. Chem. Phys., 6(15): p. 4042-4046. (2004.)
13. Dodero, G., L. De Michieli, O. Cavalleri, et al., Colloids and Surfaces A: Physicochemical and Engineering Aspects, 175(121-128). (2000.)
14. Zhang, W.W., C.S. Lu, Y. Zou, et al., Journal of Colloid and Interface Science, 249(2): p. 301-306. (2002.)
15. Uvdal, K., P. Bodö, and B. Liedberg, Journal of Colloid Interface Science, 149: p. 162. (1992.)
16. Schlaf, R., H. Murata, and Z.H. Kafafi, Journal of Electron Spectroscopy and Related Phenomena, 120(1-3): p. 149-154. (2001.)
17. Kohlscheen, J., Y.N. Emirov, M.M. Beerbom, et al., Journal of Applied Physics, 94(6): p. 3931-3938. (2003.)

18. Beerbom, M.M., Z. Bednarova, R. Gargagliano, et al., Applied Surface Science, 236(1-4): p. 208-216. (2004.)

19. Dam, N., B.V. Doran, J.C. Braunagel, and R. Schlaf, Journal of Physical Chemistry B, 109(2): p. 748-756. (2005.)

20. Dam, N., M.M. Beerbom, J.C. Braunagel, and R. Schlaf, Journal of Applied Physics, 97(2). (2005.)

21. Beerbom, M.M., R. Gargagliano, and R. Schlaf, Langmuir, 21(8): p. 3551-3558. (2005.)

22. Schreiber, F., Prog. Surf. Sci., 65: p. 151-256. (2000.)

23. Ulman, A., Chemical Review, 96(4): p. 1533. (1996.)

24. Nuzzo, R.G. and D.L. Allara, Journal of the American Chemical Society, 105: p. 4481. (1983.)

25. Vericat, C., M.E. Vela, and R.C. Slavarezza, Phys. Chem. Chem. Phys., 7: p. 3258-3268. (2005.)

26. Einstein, A., Ann. Physik, 17(132). (1905.)

27. Moulder, J.F., W.F. Stickle, P.E. Sobol, and K.D. Bomben, *Handbook of X-ray Photoelectron Spectroscopy*, ed. J. Chastain and R.C. King. 1995: Physical Electronics, Inc.

28. Siegbahn, K., *Nobel Lectures, Physics 1981-1990*, in *Nobel Lectures*, T. Frangsmyr, Editor. 1993, World Scientific Publishing.

29. Hufner, S. (2003.)

30. Hofman, P., *Mean Free Path of Electrons in a Solid*. 2004.

31. Kojima, I. and M. Kurahashi, Journal of Electron Spectroscopy and Related Phenomena, 42: p. 177. (1987.)

32. Beerbom, M.M., R. Gargagliano, and R. Schlaf, Unpublished.)

33. Uvdal, K. and T.P. Vikinge, Langmuir, 17(6): p. 2008-2012. (2001.)

34. Petoral, R.M. and K. Uvdal, Colloids and Surfaces B-Biointerfaces, 25(4): p. 335-346. (2002.)

35. Paredes Olivera, P., E.M. Patrito, and H. Sellers, Surface Science, 327: p. 330-357. (1995.)

36. Madix, R.J., Surface Science, 89: p. 540-553. (1979.)

37. Riggs, W.M. and M.J. Parker, *Surface analysis by X-ray photoelectron spectroscopy*, in *Methods of Surface Analysis*, A.W. Czanderna, Editor. 1975, Elsevier Publishing Company: Amsterdam. p. 103-158.

38. Schlaf, R., L.A. Crisafulli, H. Murata, et al. *Determination of the Electronic Structure of Organic Schottky Contacts by Photoemission Spectroscopy*. in *SPIE 44th annual meeting*. 1999. Denver, USA.

39. Zubavichus, Y., O. Fuchs, L. Weinhardt, et al., Radiat. Res., 161(3): p. 346-358. (2004.)

40. Scofield, J.H., Journal of Electron Spectroscopy and Related Phenomena, 8(2): p. 129-137. (1976.)

41. Tilinin, I.S., A. Jablonski, and W.S.M. Werner, Prog. Surf. Sci., 52(4): p. 193-335. (1996.)

42. Schlaf, R., C.D. Merritt, L.A. Crisafulli, and Z.H. Kafafi, Journal of Applied Physics, 86(10): p. 5678-5686. (1999.)

43. Gonella, G., S. Terreni, D. Cvetko, et al., Journal of Physical Chemistry B, 109: p. 18003-18009. (2005.)